JOURNAL OF GEOPHYSICAL RESEARCH, VOL. 115, B06404, doi:10.1029/2009JB006470, 2010

Low heat flux and large variations of lithospheric thickness in the Canadian Shield

F. Lévy,[1] C. Jaupart,[1] J.-C. Mareschal,[2] G. Bienfait,[1] and A. Limare[1]

Received 20 March 2009; revised 24 December 2009; accepted 13 January 2010; published 23 June 2010.

[1] Ten new heat flux determinations have been made using measurements in 22 mining exploration boreholes located at latitudes higher than 51°N in the Canadian Shield. They provide data in poorly sampled regions near the core of the North American craton where one expects the lithosphere to be thickest. The new heat flux values are all smaller than 34 mW m^{-2} and are among the lowest recorded so far in the shield. For all the new sites, there is no relationship between heat flux and heat production in surface rocks. In the Canadian Shield, heat flux variations occur at wavelengths <100 km and are mostly of crustal origin. Local averages in two 250 × 250 km windows located on Archean areas at high latitudes on either side of James Bay are 29 mW m^{-2} and 31 mW m^{-2}, the lowest values found so far at this scale in the Canadian Shield. *S* wave traveltime delays derived from tomographic models provide the additional constraints needed to resolve differences of deep lithospheric thermal structure. There is no significant correlation between average surface heat flux and traveltime delays within the Canadian Shield, confirming that variations of the surface heat flux are mostly of crustal origin. Traveltime delays cannot be explained by variations in crustal heat production only and require variations of heat supply to the lithosphere and/or radiogenic heat production in the lithospheric mantle. These variations are associated with changes of lithospheric thickness that may be as large as 80 km. The heat flux at the base of the Superior lithosphere is constrained to be 11 ± 2 mW m^{-2}.

Citation: Lévy, F., C. Jaupart, J.-C. Mareschal, G. Bienfait, and A. Limare (2010), Low heat flux and large variations of lithospheric thickness in the Canadian Shield, *J. Geophys. Res.*, *115*, B06404, doi:10.1029/2009JB006470.

1. Introduction

[2] The large thickness of continental lithosphere beneath Precambrian provinces implies changes of heat flux between oceans and continents and imposes constraints on mantle convective motions. On a smaller scale, variations of lithospheric thickness and heat flux at the base of continental roots carry information on the pattern of convection beneath continents. Such variations provide constraints on continent-forming processes in the Earth's distant past. The thick continental roots that underlie Precambrian provinces may have been generated at the time of continental crust extraction from the convecting mantle or at later times through a combination of magmatic and tectonic events. The Superior Province of the Canadian Shield, for example, which is the largest Archean province on Earth, formed through accretion of several volcanic arcs and was subjected to major thermal perturbations at the end of the Archean [*Card*, 1990; *Thurston*, 2002]. The Superior craton was welded to other Archean blocks during Proterozoic collision events that led to the present assemblage [*Hoffman*, 1989]. How much of the present thickness of the roots can be attributed to these events cannot be assessed without knowledge of their geometry beneath geological provinces of different ages.

[3] Large-scale models of the structure of continental lithosphere have been derived from global data sets. Using age as the primary control on crustal and lithospheric structure together with simple parameterizations of the relationship between values of the average heat flux at the surface and at the Moho, *Pollack and Chapman* [1977], *Rohm et al.* [2000], and *Artemieva and Mooney* [2001] found that large variations of lithosphere thickness can occur between provinces of different ages. By construction, such studies have poor resolution on the scale of an individual craton and do not account for data uncertainties. On the scale of a single continent such as North America, several seismological and magnetotelluric studies allow constraints on lithospheric temperatures and thickness [*van der Lee and Nolet*, 1997; *Jones et al.*, 2003; *van der Lee and Frederiksen*, 2005; *Pedersen et al.*, 2008]. Using tomographic models and equations for seismic *S* wave velocity as a function of pressure and temperature, *Shapiro et al.* [2004] and *Priestley and McKenzie* [2006] have derived lithospheric geotherms and maps of lithospheric thickness. To date, there has been no

[1]Équipe de Dynamique des Fluides Géologiques, Institut de Physique du Globe de Paris, Paris, France.
[2]GEOTOP, Université du Québec à Montréal, Montreal, Quebec, Canada.

0148-0227/10/2009JB006470

Table 1. New Heat Flux Measurements in the Superior Province[a]

Site and Hole	Latitude (°N)	Longitude (°W)	Dip (deg)	Δh (m)	N_k	⟨k⟩ (W m^{-1} K^{-1})	Γ (mK m^{-1})	Q (mW m^{-2})	σ_Q (mW m^{-2})	ΔQ (mW m^{-2})	Q_c (mW m^{-2})
Lagrande											**20** (B)
04-05	53°31′45″	76°33′15″	60	320–550	10	2.89	6.7	19.2	0.9	2.7	21.9
04-06	53°31′42″	76°33′49″	52	240–290	7	2.94	5.0	14.7	1.1	3.2	17.9
Eleonore											**31** (B)
05-02	52°42′05″	76°04′46″	56	390–520	9	2.47	12.4	30.7	2.0	2.1	32.8
05-03	52°42′00″	76°04′45″	58	320–610	9	2.45	11.1	27.2	2.9	2.6	29.8
Clearwater											**33** (A)
05-05	52°12′33″	75°48′38″	80	360–700	11	2.66	11.5	30.6	1.8	2.5	33.1
05-05	52°12′33″	75°48′38″	80	740–810	11	2.35	13.3	31.3	0.4	1.1	32.4
05-06	52°12′31″	75°48′23″	80	500–740	9	2.63	11.9	31.4	1.5	2.2	33.6
05-07	52°12′39″	75°48′23″	77	170–370	2	2.77	10.9	30.1	1.0	3.2	33.3
Musselwhite											**33** (A)
06-01	52°37′28″	90°23′33″	76	250–740	11	2.73	11.2	30.7	2.2	2.6	33.3
Miminiska											**34** (C)
06-02	51°34′51″	88°31′09″	45	100–215	5	3.91	6.5	25.5	2.8	8.2	33.7
06-03	51°34′51″	88°31′09″	61	180–230	3	3.91	7.4	28.8	0.5	4.9	33.7
Thierry Mine											**28** (A)
06-05	51°30′24″	90°21′11″	74	240–690	12	2.91	9.2	26.8	2.0	2.9	29.7
06-06	51°30′22″	90°21′11″	70	220–490	9	2.61	9.4	24.4	1.4	2.6	27.0
06-08	51°30′24″	90°21′11″	62	290–750	10	2.60	9.5	24.6	2.3	2.5	27.1
Raglan											**32** (B)
05-01; 06-13*	61°41′55″	73°34′50″	75	320–410	9	2.80	13.2	37.0	1.7	−5.7	31.3
06-14	61°41′50″	73°34′52″	77	340–480	9	2.70	13.3	36.2	1.3	−5.6	30.6
06-15	61°41′32″	73°34′52″	75	210–390	9	2.74	13.2	39.5	2.7	−6.1	33.4
Camp Coulon											**28** (B)
07-12	54°47′43″	71°17′09″	54	258–545	7	3.69	7.2	26.4	2.6	2.6	29.0
07-13	54°47′95″	71°17′20″	40	300–450	8	3.73	6.6	24.5	1.9	3.0	27.5
07-14	54°47′43″	71°17′34″	56	275–355			4.7				
Poste Lemoyne											**27** (C)
04-08	53°27′51″	75°12′58″	52	200–250	7	2.71	10.0	27.0	3.0	2.3	29.3
07-15	53°27′37″	75°12′21″	55	200–410	7	2.50	9.1	22.7	2.2	2.2	24.9
Corvet											**27** (B)
07-16	53°19′72″	73°55′60″	67	200–470	7	2.80	8.6	24.0	1.0	2.8	26.8

[a]Δh is the depth interval over which heat flux is estimated; k is thermal conductivity; N_k is the number of conductivity determinations (total number of samples analyzed is $5 \times N_k$, see section 2 for details); Γ is the temperature gradient; $\langle k \rangle$ is the average thermal conductivity; Q is heat flux; σ_Q is the standard deviation on the heat flux; ΔQ is the climatic correction for heat flux; and Q_c is the corrected heat flux, where boldface indicates the site-averaged corrected heat flux. Asterisk indicates a hole measured twice at a 1 year interval.

direct comparison between seismic models and thermal models derived from heat flow data. In principle, the different types of data complement one another. Seismic velocities are sensitive to temperature, composition and water content. Thus, combining seismic and heat flux constraints can narrow down considerably the range of geophysical models that are admissible [*Shapiro et al.*, 2004; *Perry et al.*, 2006b]. In addition, such comparisons allow tests of the various assumptions that go into model calculations. For example, lithospheric thermal models strongly depend on the amount and distribution of radioactive elements in the crust. Geochemical studies on the amount and distribution of radioactive elements have led to generic average crustal models in a few selected age groups [*Rudnick and Fountain*, 1995; *Rudnick and Gao*, 2003], but do not account for the large lateral variations of crustal heat production that may occur within a single province [*Jaupart and Mareschal*, 2003].

[4] Data coverage for heat flux and crustal heat production over the Canadian Shield is dense enough to contribute usefully to studies of the thick continental root that lies beneath it [*Eade and Fahrig*, 1971; *Jessop and Lewis*, 1978; *Fountain et al.*, 1987; *Shaw et al.*, 1994; *Perry et al.*, 2006a]. In order to determine lateral temperature changes in a continental root, however, one must determine the heat flux at the base. This basal heat flux is probably as low as 15 mW m^{-2} [*Mareschal and Jaupart*, 2004]. Thus, even changes that are large in proportion of such a small value are difficult to determine from surface heat flux data because they are overwhelmed by variations of crustal heat production. Basal heat flux variations of ±3 mW m^{-2} (about 20% of the average) pale in comparison to variations of the surface heat flux that are as large as 20 mW m^{-2} in the Canadian Shield. In order to resolve variations of lithospheric thickness and convective heat supply, surface heat flux measurements must be supplemented by other geophysical data. In the Superior Province, with few exceptions, heat flux measurements so far have only been made in areas south of 50°N due to the vagaries of drilling for mineral exploration, difficult access, and the presence of permafrost. Yet, seismic studies indicate that the continental lithosphere is coldest and thickest in the northern parts of the province, above the 50°N parallel [*Shapiro et al.*, 2004; *van der Lee and Frederiksen*, 2005]. The present study was undertaken to reduce the heat flux data gap in order to allow comparisons with seismic observations over a large part of the North American craton.

[5] In this paper, we report on ten new surface heat flux determinations based on measurements in 22 deep boreholes located at latitudes higher than 50°N in the Canadian Shield. We also report on measurements of radiogenic heat production in shallow crustal rocks at all the measurement sites. We

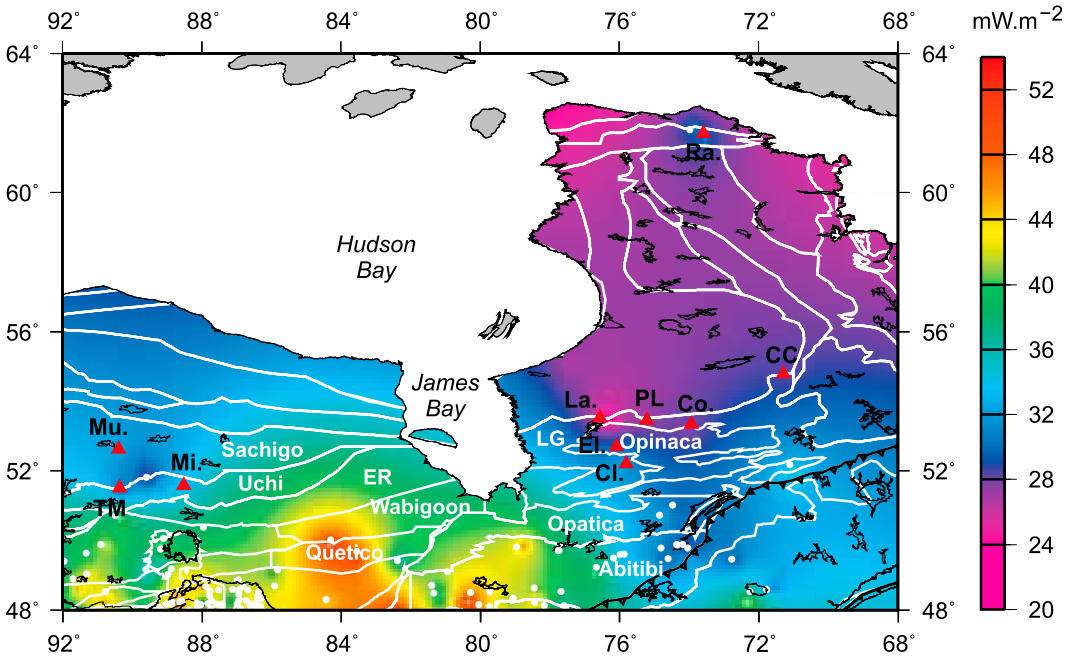

Figure 1. Heat flux map of the northern Superior Province. Red triangles represent the new heat flux sites. White dots are previous measurement sites. White lines mark subprovince boundaries. Subprovince names are in white (ER, English River belt; LG, La Grande belt), and site names are in black. See Tables 1 and 2 for full site names and descriptions.

took special care to make several measurements in two areas of limited horizontal extent in order to evaluate possible biases due to anomalous terranes. This allows us to estimate local averages of heat flux and temperature gradient which can be downward continued to large lithospheric depths. We find that the locally averaged heat flux is much lower in the northernmost parts than in southern part of the Superior Province. We then use seismic *S* wave traveltimes derived from the CUB2.0 model of *Shapiro and Ritzwoller* [2002] and the NA04 model of *van der Lee and Frederiksen* [2005] to evaluate the magnitude of heat flux variations at the base of the lithosphere. We calculate vertical temperature profiles through the lithosphere that are consistent with both the surface heat flux data and constraints on the Moho heat flux. These geotherms depend on the basal heat flux and allow predictions of seismic traveltimes that are compared to the data. We find that the Moho heat flux cannot be laterally uniform in the Canadian Shield and that it may vary by as

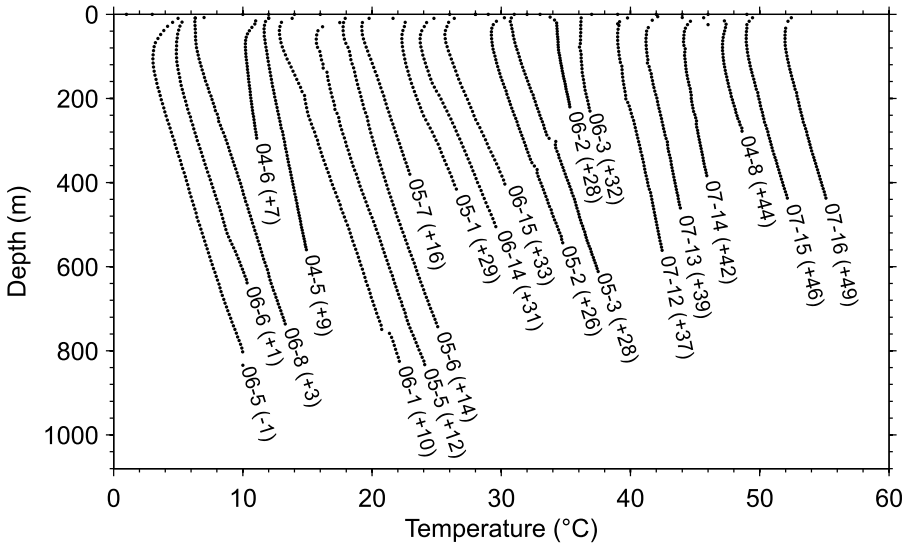

Figure 2. Temperature-depth profiles for all the new sites reported in this study. The profiles are shifted horizontally as indicated (in °C) to avoid superposition.

Table 2. Site Description of New Heat Flux Measurements

Borehole		Geological Unit		
Number	Name	Region	Age	Site Description
05-01	Raglan	Cape Smith Fold Belt	Proterozoic	Holes through thick permafrost; mafic to ultramafic intrusives and flows with altered contacts.
06-15	Raglan			
06-14	Raglan			
06-13	Raglan			Same hole as 05-01; repeat measurement at a 1 year interval to check for thermal stability.
04-05	LaGrande	LaGrande volcano-plutonic belt	Archean	Granite intrusion within volcanic and sedimentary sequence.
04-06	LaGrande			
04-08	Poste Lemoyne	LaGrande Belt	Archean	Basaltic flows.
07-15	Poste Lemoyne			
05-02	Eleonore	LaGrande Belt	Archean	Sedimentary sequence against diorite-tonalite pluton; close to boundary between La Grande and Opatica Belts.
05-03	Eleonore			
07-12	Camp Coulon	LaGrande Belt	Archean	Volcano-sedimentary sequence; mafic volcanics/felsic pyroclastics.
07-13	Camp Coulon			
07-16	Corvet	LaGrande Belt	Archean	Basaltic flows.
05-05	Clearwater	Opinaca Belt	Archean	Tonalite intrusion and Eau Claire volcaniclastic formation.
05-07	Clearwater			
05-08	Clearwater			
06-01	Musselwhite	Sachigo subprovince	Archean	Within North Caribou greenstone belt; mafic volcanics and altered schist sequence.
06-02	Miminiska	Uchi Belt	Archean	Volcanics and sedimentary rocks.
06-03	Miminiska			
06-04	Thierry Mine	Uchi Belt	Archean	Granite intrusion within mixed volcanics sequence.
06-05	Thierry Mine			
06-06	Thierry Mine			

much as ±3 mW m^{-2}. The analysis leads to constraints on the heat flux at the base of the Canadian lithosphere.

2. New Heat Flux and Heat Production Measurements

[6] Measurement techniques have been described in previous papers [*Mareschal et al.*, 1989; *Pinet et al.*, 1991] and are summarized in Appendix A. Recent variations in surface temperature due to climate change, and lateral variations in thermal conductivity or in surface boundary conditions, due for example to the numerous lakes that dot the Canadian Shield, outweigh the effect of the vertical variations in thermal conductivity. Therefore, we strived to find deep boreholes (500 m) or, where they were not available, to make measurements in neighboring boreholes. Following previous studies [*Pinet et al.*, 1991], our heat flux determinations are rated from A to C depending on the borehole characteristics and data consistency (Appendix A). As regards thermal conductivity determinations, the guiding principle is that we seek values that are representative of the bulk rock average. One single measurement on a thin disk is likely to depend on the local mineral composition, which may vary on the scale of individual minerals. Therefore, for each piece of core, we measure the conductivities of five samples with different thicknesses in order to determine a conductivity value that is independent of scale. One additional advantage of this technique is that it eliminates the contact resistance between the rock sample and the measurement device, which may vary from sample to sample. For these reasons, the number of conductivity values listed in Table 1 does not reflect the reliability of our estimates. The robustness of our estimates depends on the total number of individual conductivity measurements made at each site, which typically involves two boreholes or more. In this study it is never less than 35 and may reach 165.

[7] The new site locations and the vertical temperature profiles obtained in this study are shown in Figures 1 and 2.

Table 3. Heat Production at New Heat Flux Sites in the Superior Province[a]

Site	Lithology	U (ppm)	Th (ppm)	K (%)	A (μW m^{-3})	σ_A (μW m^{-3})	N_A
LaGrande	granodiorite	0.22	0.40	0.89	0.17	0.04	17
Eleonore	wacke	1.45	5.53	2.20	0.96	0.27	20
Clearwater	mafic volcaniclastics	0.79	2.78	1.00	0.49	0.31	21
Musselwhite	gneiss	0.69	2.20	2.62	0.57	0.10	7
Miminiska	graywacke	1.63	5.43	2.16	0.98	0.19	11
Thierry Mine	granite	2.43	9.77	2.33	1.52	0.77	13
Raglan	mafic volcanics	0.19	0.63	0.23	0.11	0.08	12
Camp Coulon	rhyolite	2.01	10.13	2.19	1.42	0.23	7
Poste Lemoyne	mafic volcanics/sediments	0.53	1.87	0.98	0.36	0.35	7
Corvet	intermediate volcanics	0.94	4.06	0.90	0.60	0.17	5

[a]U, Th, and K are uranium, thorium, and potassium concentrations; A is heat production; σ_A is standard deviation; and N_A is the number of samples.

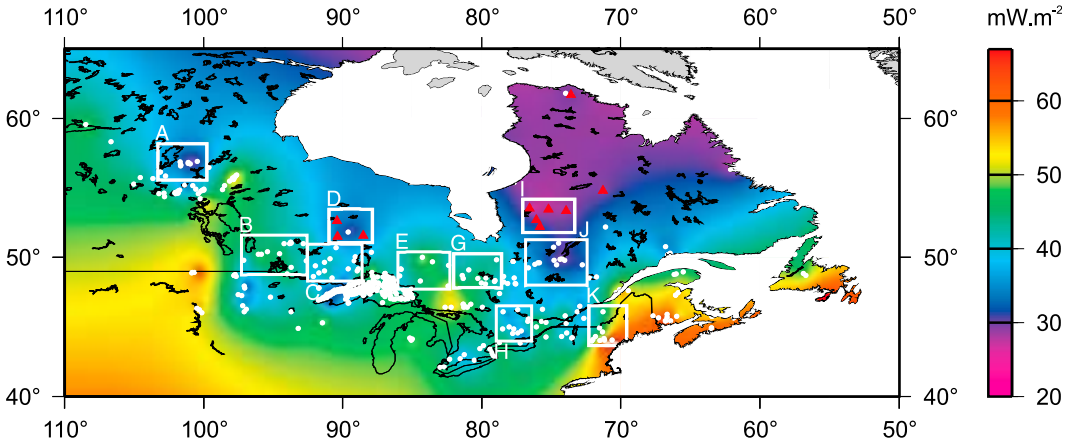

Figure 3. Heat flux map of the Canadian Shield. Red triangles represent the new measurement sites, and white dots are measurement sites from previous studies. The white frames show the locations of ten averaging windows selected using criteria that are detailed in section 2.1.

Borehole characteristics are described in Table 2. The new heat flux and heat production data are summarized in Tables 1 and 3.

2.1. Overview of the New Heat Flux Data

[8] Special care was taken to obtain reliable measurements at the northernmost site located at 61°N within a thick (>500 m) permafrost region near Hudson Strait in northern Quebec. At this remote site, which is close to the Raglan mine, a tube filled with silicone oil was emplaced in a hole immediately after drilling. Because thermal reequilibration in permafrost is delayed by latent heat effects, we logged the temperature in the hole two and three years after drilling was completed to verify that thermal stability had been reached. Two other holes containing ice slurry (the brine used during drilling) could be penetrated and were logged to evaluate small-scale horizontal variations of thermal structure [*Chouinard et al.*, 2007]. After the correction for the glacial retreat, we obtain a value of 31 mW m^{-2} for heat flux. Our site is located about 30 km away from an older measurement site, Asbestos Hills [*Taylor and Judge*, 1979]. For the latter site, *Taylor and Judge* [1979] tried several climate corrections based on different assumptions on the temperature at the base of the Laurentide ice sheet (see Appendix A). With assumptions similar to ours, they obtained a value of 28 mW m^{-2}.

[9] The other new sites of this study can be split in two geographical groups. One group, west of James Bay, straddles the Uchi and Sachigo belts of the western Superior Province (Figure 1). There, the new data complement one older measurement at the Otoskwin River site [*Jessop and Lewis*, 1978]. They confirm that the surface heat flux is low in that area, with a local average of 31 mW m^{-2}. The other group, east of James Bay, is located in and around the Archean LaGrande volcano-plutonic belt which lies to the north of the Opatica belt [*Card*, 1990]. The LaGrande belt may be related to the Uchi and English River belts of the western Superior Province. Five measurements <100 km apart define a low heat flux area with an average of 29 mW m^{-2}. The heat flux at the LaGrande site, 20 mW m^{-2}, is the lowest value recorded so far in the Canadian Shield. Farther to the northeast, one new heat flux measurement within the same belt, at Camp Coulon, is also low (28 mW m^{-2}).

[10] In the Superior Province, the new heat flux data add nine values to the data set of *Perry et al.* [2006a]. They represent only 11% of the total number of values available in the Province, and hence do not significantly affect the bulk statistics. The province-wide average is now 40 mW m^{-2} instead of the previous estimate of 41 mW m^{-2} [*Perry et al.*, 2006a]. The new data have been included in a heat flux map (Figure 1). With the uneven distribution of heat flux sites and the large contrasts that are observed in a few isolated areas, the map must be considered as an approximation and is only presented to illustrate the heat flux variations in the Province. The new measurements confirm the low heat flux in the northern part of the shield that was previously extrapolated from a few scattered measurements. This is now the largest low heat flux area in North America. The trend of decreasing heat flux toward the north and toward the center of the shield was already apparent in the data set of *Perry et al.* [2006a] but was somewhat obscured by the juxtaposition of volcano-plutonic and volcano-sedimentary belts with contrasting heat production rates. This trend may appear as part of a larger-scale pattern over the whole North American continent [*Blackwell and Richards*, 2004]. This continent-wide pattern, which is defined mostly by the contrast between low heat flux of the Canadian Shield and the high values in the younger geological provinces to the south, reflects the history of continental accretion.

[11] In order to better understand the heat flux trend within the Canadian Shield, one must account for small-scale fluctuations due to changes of crustal heat production. The main problem is due to the large heat flux anomalies over enriched granitic plutons [*Jessop and Lewis*, 1978]. These plutons are usually of small size, and the local heat flux value is not representative of the average crust in a province. To alleviate this potential problem, we have averaged heat flux values over ten geographical windows (Table 4 and Figure 3). Window selection was based on the following criteria: they must be large enough and include enough heat flux values to allow the smoothing of small-scale variations, and they must be distributed over the whole shield. We discuss the signifi-

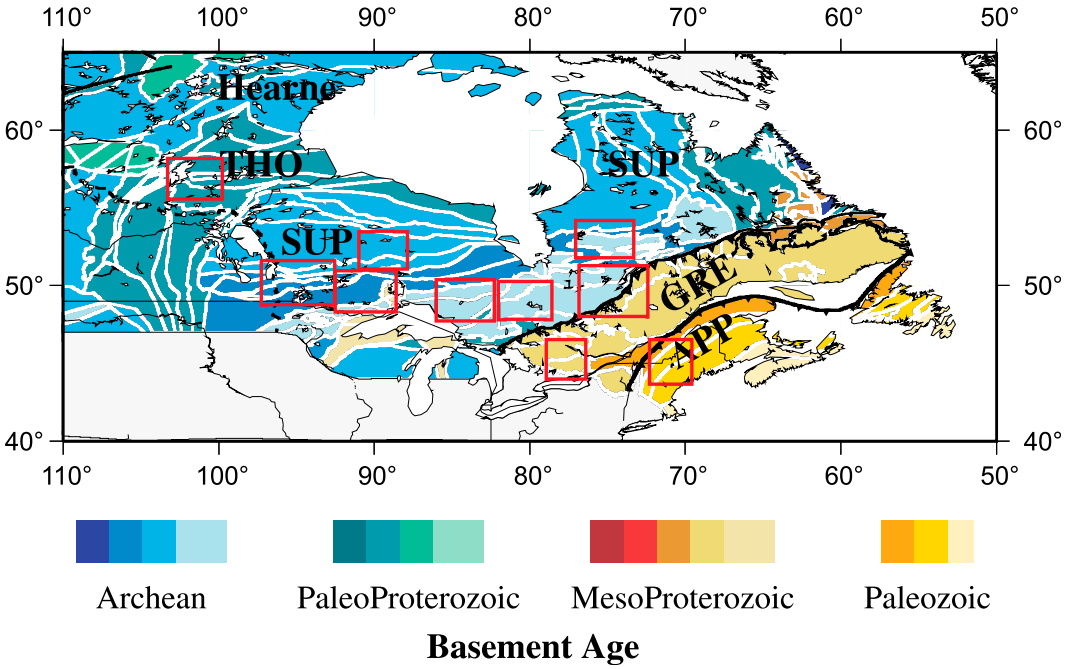

Figure 4. Geological map of the Canadian Shield, showing the major geological provinces. THO is the Trans-Hudson Province, SUP is the Superior Province, GRE is the Grenville Province, and APP is the Appalachians. Red frames show the locations of the ten windows in Figure 3.

cance and reliability of local averages later in the paper in connection with study of seismic anomalies. The size of all the windows selected is never less than 200 km (Table 4). Two windows (labeled D and I, Table 4) have a small number of heat flux data but they correspond to areas where the heat flux is uniformly low and the average cannot be biased by isolated enriched plutons. As explained above, one additional heat flux determination to the northeast of window I, at the Camp Coulon site, confirms that the heat flux is low in that part of the shield. In fact, the Camp Coulon heat flux value is identical to the window average within measurement error. Data for the ten windows selected here will be discussed later in the paper when they will be used to calculate lithospheric geotherms. For the moment, we focus on windows I and D in the Superior Province which include the new data (Figures 3 and 4). The LaGrande window I and the western Superior window D have the lowest averages (29 mW m^{-2} and 31 mW m^{-2}, respectively). Both values are at least 10 mW m^{-2} lower than those in the southern part of the province.

2.2. Heat Flux and Heat Production

[12] The measurement sites of this study involve both mafic volcanic assemblages and chemically evolved rocks such as granites. The granodiorite samples from the LaGrande site stand out with surprisingly low uranium and thorium concentrations, and radiogenic heat production, in contrast to similar plutons in the Wawa or Abitibi belts farther south. The large variations of surface heat production between the sites are not reflected in the heat flux values. All the new values are less than 34 mW m^{-2}, i.e., significantly below the Superior Province wide average of 40 mW m^{-2}.

Table 4. *S* Wave Vertical Traveltime Delay and Heat Flux Data for the Ten Windows of Figures 3 and 6[a]

Window	Latitude (°N)	Longitude (°W)	$\Delta X_{Lat} \times \Delta Y_{Lon}$ (km × km)	Province	$\overline{\Delta t_s}^{VDL}$ (s)	$\overline{\Delta t_s}^{SR}$ (s)	N	$\overline{Q}$ (mW m^{-2})	σ_Q (mW m^{-2})	$\bar{A}$ (μW m^{-3})	σ_A (μW m^{-3})
A	56°52′	101°31′	290 × 213	THO	−1.44	−3.13	11	32.1	1.7	0.68	0.12
B	50°11′	94°55′	316 × 335	SUP	−1.76	−2.47	14	43.6	1.9	1.19	0.35
C	49°38′	90°33′	297 × 281	SUP	−1.66	−2.28	13	40.6	1.3	0.64	0.18
D	52°31′	89°26′	323 × 209	SUP	−1.29	−2.18	4	30.5	1.7	0.67	0.19
E	49°03′	84°09′	297 × 273	SUP	−1.46	−1.76	9	46.1	2.8	0.89	0.21
G	49°03′	80°18′	273 × 252	SUP	−1.50	−1.46	10	42.9	1.7	0.64	0.16
H	45°15′	77°39′	284 × 199	GRE	−0.48	−1.26	10	38.9	3.5	0.47	0.30
I	52°59′	75°11′	266 × 250	SUP	−1.76	−2.10	5	28.7	1.6	0.48	0.15
J	49°38′	74°37′	364 × 320	GF	−1.49	−1.48	13	31.1	1.0	0.42	0.09
K	45°05′	70°56′	318 × 215	APP	+0.13	−1.25	10	57.3	5.8	2.60	0.27

[a]Latitude and longitude refer to center of cell. ΔX_{Lat} and ΔY_{Lon} are the window dimensions in the vertical (latitude) and horizontal (longitude) directions. $\overline{\Delta t_s}$ is the mean *S* wave vertical traveltime delay from 60 to 300 km, for *van der Lee and Frederiksen* [2005] (VDL) and *Shapiro and Ritzwoller* [2002] (SR). *N* is the number of heat flux measurements averaged by box, $\overline{Q}$ is the mean surface heat flux, and σ_Q is the standard error on $\overline{Q}$. $\bar{A}$ is the mean heat production, and σ_A is the standard error on $\bar{A}$. Provinces are as follows: THO, Trans-Hudson Orogen; SUP, Superior; GF, Grenville Front (Superior-Grenville); GRE, Grenville; APP, Appalachians.

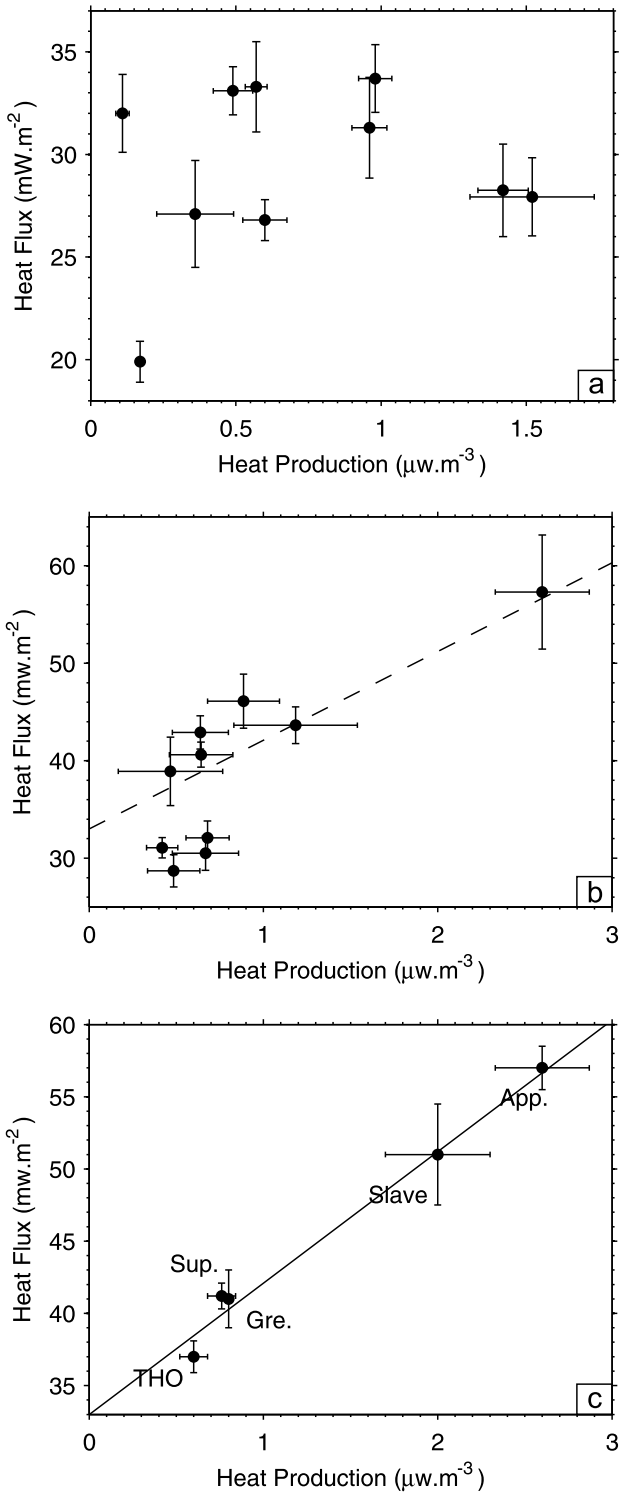

Figure 5. (a) Surface heat flux versus surface heat production for all the new measurement sites. (b) Relationship between the local averages of surface heat flux and heat production for the ten windows in Figure 3. Dashed line is the best fit linear relationship for the province-wide averages. (c) Relationship between province-wide averages of heat flux and heat production for major geological provinces of North America [from *Perry et al.*, 2006a]. Line shows the best fit linear relationship with a slope of 9.1 km and a heat flux intercept of 33 mW m^{-2}.

[13] Low heat flux values can be explained in two different ways: low heat flux at the base of anomalously thick lithosphere or depletion of radioactive elements in the crust. For the lithosphere of the Canadian Shield which is thicker than 200 km [*Rudnick and Nyblade*, 1999], differences in thickness induce variations of surface heat flux over very long wavelengths (>≈500 km [*Mareschal and Jaupart*, 2004]). This is not consistent with the data, which vary by relatively large amounts over distances less than 250 km, between windows C and D for example. We do not rule out variations of lithospheric thickness or heat flux at the base of the lithosphere, and in fact shall determine their magnitude later in the paper. Such variations, however, can only account for a small fraction of the changes that are recorded in surface heat flux data. We therefore conclude that the low heat flux values reported in this paper are due to depleted crust.

[14] The measurement sites are not systematically associated with low surface heat production, as shown by the Thierry Mine boreholes which intersect an enriched granite. Figure 5a emphasizes the lack of correlation between surface heat flux and heat production values at the new sites. This does not come as a surprise and has been observed in all the provinces of the Canadian Shield [*Mareschal et al.*, 1999]. This is in marked contrast with many younger provinces where enriched plutons intrude older rocks with lower heat production. The southern Superior Province is characterized by thick volcanic packages emplaced on top of basement that may not be much older than them. In such conditions, surface heat production contrasts tend to be small and heat flux variations are mostly due to changes of composition in the basement that are not necessarily reflected in the surface rocks, as illustrated in the Abitibi province [*Pinet et al.*, 1991]. The new data are remarkable because they are so uniform: with the exception of the LaGrande site, they are all within a tight range of 27–34 mW m^{-2}. This is best interpreted as a background heat flux over poorly differentiated crust slightly and locally modified by thin superficial units. Using the Moho heat flux estimate of 15 mW m^{-2} from *Perry et al.* [2006a], the average crustal heat production in 40 km thick crust with a heat flux of 29 mW m^{-2} is 0.35 μW m^{-3}, much lower than the average Archean crust (0.65 μW m^{-3} [*Jaupart and Mareschal*, 2003]). This is within the range of heat production values for granulite facies terranes, which have the lowest heat production among continental crustal material [*Rudnick and Fountain*, 1995]. The very low heat flux at the LaGrande site can only be interpreted as due to anomalously large amounts of undifferentiated mafic rocks in the crustal column. It also provides a strong constraint on Moho flux which must be less than 20 mW m^{-2}.

[15] Using the average values for the ten windows of Table 4, a relationship between heat flux and heat production begins to emerge (Figure 5b). These data can be evaluated using the large-scale systematics of heat flux and heat production in North America. *Perry et al.* [2006a] considered the average heat flux and surface heat production in five geological provinces covering the geological history of the stable continent and representing different types of continental crust. With province wide averages, they obtained values that are not affected by isolated anomalies and include different rock types. All provinces have been extensively deformed and eroded, so that rocks from a large range of depths can be found at the surface. The metasedimentary-

plutonic belts of the western Superior Province, for example, include rocks from all metamorphic grades up to granulite facies. The province-wide averages exhibit a remarkable linear relationship, with a heat flux intercept of ~33 mW m^{-2} corresponding to crust with zero surface heat production (Figure 5c). The value of this intercept is slightly higher than the local average values in the two northern Superior windows I and D discussed earlier and in window J adjacent to window I to the south. According to the analysis of crustal structure by *Perry et al.* [2006a], compared to the Superior Province as a whole, these northern windows can be interpreted as extreme cases with depleted crust and almost no internal crustal stratification, i.e., with little difference between upper and lower crust. It is significant that, over the large area encompassed by windows I and J, heat production values are low and vary by small amounts, and further that the mean and standard deviation of heat production are essentially the same in both windows. This confirms the lack of crustal differentiation in the area. Save for window A located in the Trans-Hudson Orogen, the data for the other windows lie close to the best fit linear relationship for the province-wide averages (Figure 5b). For the window averages, the quality of the fit is clearly not as good as that for the province-wide averages, which we attribute to insufficient sampling of heat production. A single heat flux value is sensitive to crustal heat production over large horizontal distances [*Jaupart and Mareschal*, 2003] and hence records the contribution of many different geological units. In order to obtain a representative average, more samples are needed for heat production than for heat flux. Consider for example window H in the Grenville Province, which we shall study in more detail below. Its heat flux–heat production pair of (39 mW m^{-2}, 0.47 μW m^{-3}) is slightly offset from the linear relationship. In comparison, the province-wide averages are 41 mW m^{-2} and 0.80 μW m^{-3} [*Perry et al.*, 2006a]. The heat flux is barely affected by the change of window size, whereas the heat production almost doubles. For window A in the Trans-Hudson Orogen, the problem of determining a reliable heat production average is acute due to the intricate assemblage of many belts of different origins and compositions.

[16] Two conclusions can be drawn from this analysis. One is that there seems to be two types of crustal structure in the Canadian Shield. In the northern part of the Superior Province, the crust is not well differentiated and lacks enriched upper crustal rocks. The crust found in the southern part of the Superior Province and in the other provinces has radiogenic upper crustal rocks over a thickness of ≈9 km on average lying above depleted rocks. The other conclusion is that the windows in Table 4 (≈250 km × 250 km on average) allow determinations of average heat flux that are representative of the local crust.

3. Variations of Heat Flux and Deep Lithospheric Thermal Structure

[17] In order to investigate the deep thermal structure of the lithosphere, we combine the surface heat flux with seismic data. The interest of such an approach has already been demonstrated by previous studies. For instance, *Shapiro et al.* [2004] have shown that including heat flux constraints narrows down the range of acceptable solutions in the Monte Carlo inversion of surface wave data. These authors excluded seismic models with velocities at the Moho that were not consistent with constraints on temperature deduced from heat flux data. Interestingly, the excluded models had negative temperature gradients, and hence could also have been rejected on grounds of physical implausibility. In another study, *Perry et al.* [2006b] obtained robust constraints on the Moho heat flux beneath the Superior Province by combining P_n velocities with Moho temperatures deduced from surface heat flux values. One advantage is that P_n velocities are determined locally from seismic refraction surveys, and hence are not affected by the spatial smoothing inherent to tomographic techniques. This study also yielded information on the composition of the shallow lithospheric mantle. These two studies illustrate how the combination of heat flux and seismic data improves both the thermal and seismological models.

[18] Here we generalize this approach to a large part of the Canadian Shield. We could not rely on P_n studies because there are only a few seismic refraction lines in the shield. We could not use teleseismic body wave data either because of the small number and uneven distribution of the permanent or semipermanent seismic stations that have been deployed. Thus, we chose to work with large-scale surface wave tomography models and have selected two recent ones in order to assess the robustness of the solutions. We used the CUB2.0 global model of *Shapiro and Ritzwoller* [2002] and the NA04 North American model of *van der Lee and Frederiksen* [2005]. These two models differ in many aspects including the number of seismograms analyzed and the inversion methodology. The CUB2.0 anisotropic model provides *Sv* and *Sh* shear wave velocity profiles to a depth of 400 km over a 2° × 2° grid [*Shapiro and Ritzwoller*, 2002], whereas the NA04 model provides isotropic values on a 0.5° × 0.5° grid through the upper mantle and transition zone, but the true spatial resolution is much worse (see below).

[19] We do not use the full seismic velocity profiles and prefer to use a single datum such as the traveltime delay instead, because it is more robust to the inversion procedure, as errors within one depth range are compensated by deviations in other depth ranges. In addition, this allows a straightforward comparison between different regions. Likewise, heat flux values contain less uncertainty than vertical temperature profiles due to imperfect knowledge of the input parameters entering the thermal calculations. Thus, in a first step, we compare heat flux values and traveltime delays because they are two raw indices of thermal structure if compositional effects are accounted for. We later examine in section 4 how to improve our knowledge of the heat flux at the base of the lithosphere. For this purpose, we determine vertical temperature profiles from the heat flux and calculate the implied seismic velocities and traveltime delays using the equations of *Goes et al.* [2000].

[20] For a meaningful analysis, one must ensure that the seismic and thermal data are determined on similar horizontal scales. The two types of data differ strongly in that aspect. Seismic velocity anomalies are derived by inversion using theoretical models for wave propagation through heterogeneous media that are only approximate. Thus, the true spatial resolution of the seismic models cannot be determined rigourously because it depends both on the as yet unknown structure of the crust and lithospheric mantle and on the distribution of seismic events and seismic stations. Heat flux

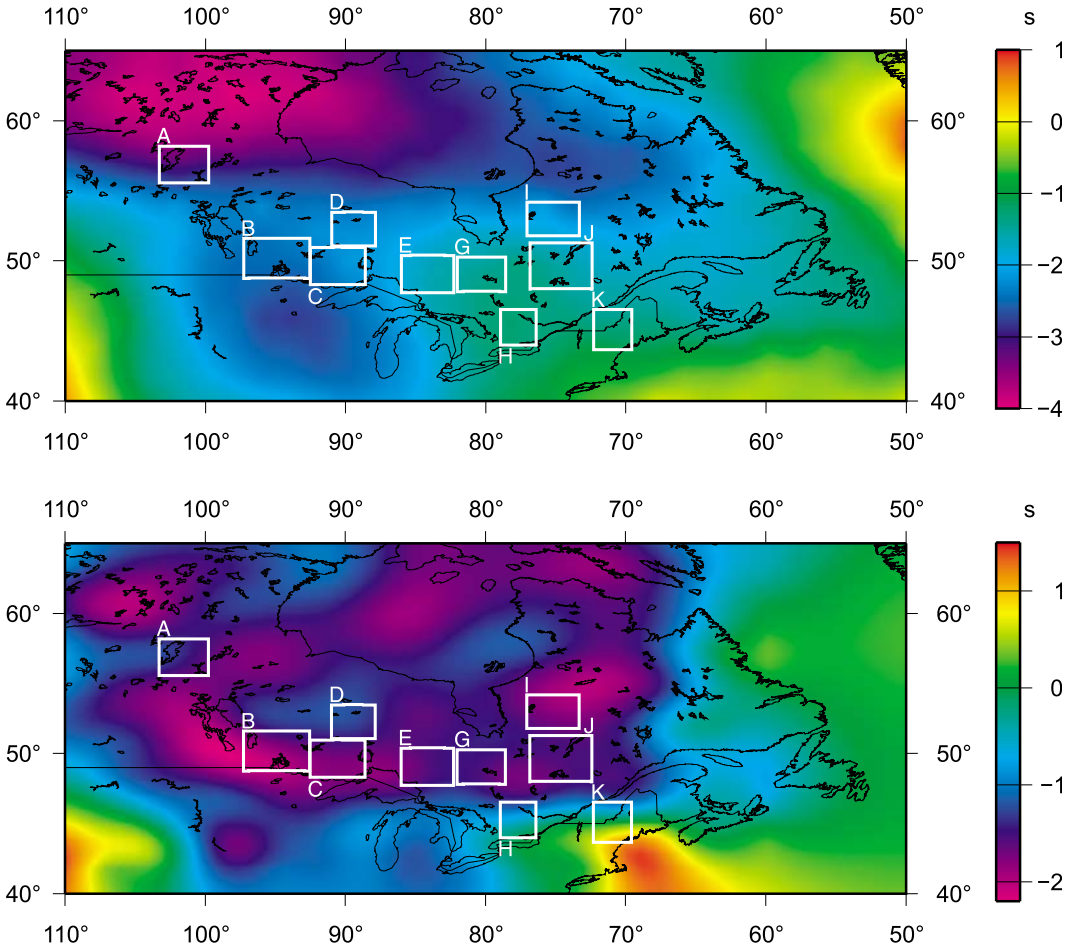

Figure 6. Maps of *S* wave vertical traveltime delays for the depth interval 60–300 km from (top) the global CUB2.0 tomographic model of *Shapiro and Ritzwoller* [2002] and (bottom) the North American NA04 model of *van der Lee and Frederiksen* [2005]. The white frames indicate the locations of the ten windows in Figure 3.

data are local measurements unevenly distributed through the shield that are very sensitive to radiogenic heat production in the crust. Downward continuation of temperature to the base of the lithosphere is feasible only if small-scale variations of shallow origin have been smoothed out.

3.1. Local Averages of Traveltime Delays

[21] The spatial resolution of the seismic data is estimated to be about 350 km and 200 km in the CUB2.0 and NA04 models, respectively, and the depth resolution is about 50 km for both [*Shapiro and Ritzwoller*, 2002; *Goes and van der Lee*, 2002; *van der Lee and Frederiksen*, 2005]. *Shapiro and Ritzwoller* [2002] estimate that the CUB2.0 model has an error of about 25 m s^{-1} (≈0.5%) in the lithospheric mantle. In the NA04 model, the amplitude of velocity anomalies is well recovered in the upper 250 km and damped at larger depths [*Goes and van der Lee*, 2002]. Resolution is commonly assessed using a checkerboard test, such that step changes of velocity over a set of adjacent squares are recovered with the available ray coverage. This is appropriate for the detection of discontinuities associated with tectonic boundaries and fossil mantle structures such as subducted slabs for example, but not for gradual changes of thermal structure across a single tectonic unit, which are our present concern. We assess the reliability of the data in two different ways, through an analysis of the average value in windows of different sizes and through a comparison of three independent data sets. Figure 6 shows maps of the traveltime delays calculated between depths of 60 and 300 km (this choice will be discussed below) for the two surface wave tomographic models. The seismic anomalies are calculated with respect to different reference models and absolute values cannot be compared: one should only pay attention to differences. The two surface wave models share many features, with a fast region over most of the shield that extends to the southeast in a wide corridor. The range of the delay variations is the same in both maps (≈3 s in the shield). There are some differences between the two models. The NA04 model shows sharper gradients at the edge of the fast central shield region. Furthermore there are differences in the anomaly pattern at an intermediate scale. For example, a wedge of slightly slower anomalies beneath James Bay, well defined in the CUB2.0 map, is absent from the NA04 one. The overall impression is that the CUB2.0 map is a blurred version of the NA04 one. In addition, we compare in Table 5 traveltime delays from the tomographic models with the few available teleseismic body

Table 5. Traveltime Delays From Two Tomographic Models and From a Body Wave Analysis at the Same Sites[a]

	Latitude (°N)	Longitude (°W)	$\overline{\Delta t_s}^{VDL}$ (s)	$\overline{\Delta t_s}^{SR}$ (s)	$\overline{\Delta t_s}^{WB}$ (s)
Flin Flon	54	100	−1.64	−2.35	−1.62
Poste à la Baleine	55	77	−1.74	−2.42	−1.78
Churchill	58	94	−1.56	−3.30	−1.49
Baker Lake	64	96	−1.15	−3.78	−1.42
Ottawa*	45	76	−0.08	−1.33	+0.63
Thunder Bay*	49	90	−1.72	−2.24	−0.07

[a]Tomographic models are those of *van der Lee and Frederiksen* [2005] and *Shapiro and Ritzwoller* [2002]. Body wave delays are from *Wickens and Buchbinder* [1980] (WB). Asterisks indicate sites with a thick sedimentary cover.

wave delays of *Wickens and Buchbinder* [1980]. The latter data include traveltimes through the crust, which is likely to induce significant differences between areas with and without a sedimentary cover. Once this is accounted for, the *Wickens and Buchbinder* [1980] values are found to be in remarkable agreement with those of the NA04 model. They are consistent with the CUB2.0 values in only two areas (Flin Flon and Poste à la Baleine). This suggests that NA04 has better resolution in the Canadian Shield.

[22] We have investigated how the NA04 traveltime delays vary with the size of the averaging window. For area I in the Superior Province, the traveltime delay is almost unaffected by the window size. Increasing or decreasing the window size by one or two degrees in latitude and longitude changes the average traveltime by less than 0.1 s. For area H in the Grenville Province at the edge of the fast central shield region, the traveltime value changes slightly with the size of the averaging window, as expected in a region with a sharp gradient. Enlarging the window size by one degree changed the delay by less than 0.2 s.

[23] The traveltime delays in Figure 6 have been calculated over the 60–300 km depth interval. We expect that traveltime anomalies are restricted to the lithosphere and the underlying thermal boundary layer and that no variations exist in the well-mixed convecting mantle. It follows that no traveltime differences originate deeper than the thickest lithospheric root. We have compared the delay difference between windows I and H for intervals between 60 km and a variable depth z_b (Figure 7). By construction, the delay is zero for z_b = 60 km. The result exhibits a remarkable systematic trend, such that the rate of increase of Δt systematically decreases with increasing z_b. For the purposes of discussion, we have drawn three lines of constant slope through the data, with breaks at depths of 120 and 300 km. We note that the rate of change becomes small below 300 km. For a total traveltime of about 50 s through 250 km thick lithosphere and an uncertainty of ≈0.5%, as discussed above, differences of ≈±0.1 s are not significant. This indicates that traveltime differences originating from below 300 km are too small to be resolved (Figure 7). Throughout the following, we shall therefore consider traveltime anomalies over the 60–300 km depth interval. Were we to adopt a smaller interval, we would take the risk of truncating part of the lithosphere. With a much larger depth interval, we might include deep anomalies unrelated to lithospheric structure and composition or perhaps noise in the data. In fact, the heat flux data will allow us to verify that lithospheric anomalies are shallower than 300 km.

3.2. Spatial Resolution of Heat Flux Data

[24] For heat flux data, the resolution problem is completely different and stems from the uneven sampling in the highly heterogeneous crust of North America. Here spatial resolution refers to the horizontal scale at which heat flux data allow determination of deep variations of thermal structure. For the purposes of calculating lithospheric geotherms, one must use heat flux averages that are not biased by small-scale features such as granitic plutons and narrow enriched plutonic-metasedimentary belts. For the size of such objects (<10–100 km), the heat flux anomalies get smoothed out by diffusion when downward continued and they do not affect deep lithospheric structure. These anomalies are due to isolated geological structures and are not representative of the average crust in a province. Inadequate sampling, however, may increase the average heat flux value. We have shown above that the ten windows of Table 4 provide adequate sampling. We used two approaches to estimate the scale at which the heat flux data can resolve variations of lithospheric thickness.

[25] The surface heat flux may be written as the sum of a crustal component and the Moho heat flux, which in turn depends on heat production in the lithospheric mantle and on the heat supplied to the lithosphere by the convecting mantle. Because of horizontal diffusion, variations of deep thermal structure get smoothed out and can only be detected at large scales. Using the analysis of *Mareschal and Jaupart* [2004] for an average lithospheric thickness of 250 km, variations of the basal heat flux over wavelengths smaller than 500 km are not detectable in the surface heat flux. For heat production in the lithospheric mantle, the effect of lateral heat diffusion is less pronounced because anomalies are generated over a large depth range including the shallow mantle. However, the changes are small due to the depleted

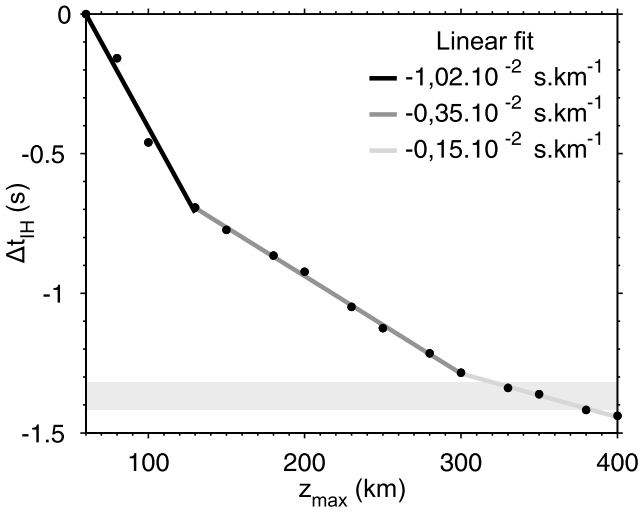

Figure 7. Traveltime difference between windows I and H from the NA04 model [*van der Lee and Frederiksen*, 2005] between depths z = 60 km and $z = z_b$ as a function of z_b. The data can be fit with three lines of constant slope.

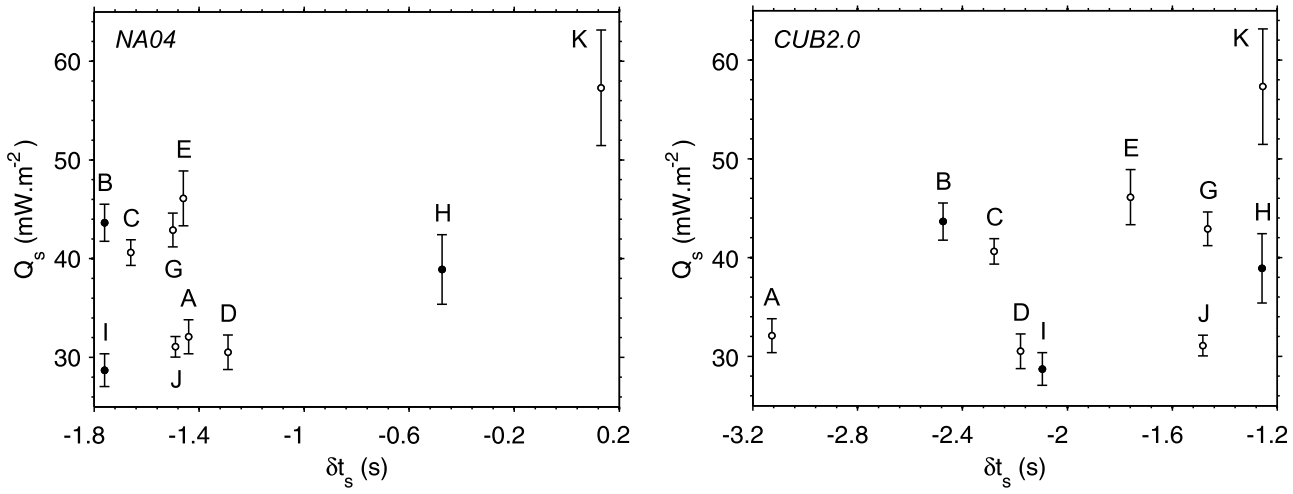

Figure 8. Mean surface heat flux and mean *S* wave vertical traveltime delay for the ten windows of Figures 3 and 6. Traveltime delays are (left) from the NA04 model of *van der Lee and Frederiksen* [2005] and (right) from the CUB2.0 model of *Shapiro and Ritzwoller* [2002].

nature of mantle rocks [*Rudnick et al.*, 1998], so that variations over wavelengths of 500 km or less are also below the detection threshold of surface heat flux measurements. For example, the change of average heat flux from window C to window D (41 to 31 mW m^{-2}) in the western Superior Province occurs over a distance of about 500 km and hence cannot be attributed to variations of the Moho heat flux. Over wavelengths longer than 500 km, variations of the Moho heat flux may be detectable if one can separate them from changes of crustal heat production.

[26] Similar conclusions can be drawn from a global analysis of the scale of heat flux variations over the shield. To this aim, *Mareschal and Jaupart* [2004] have paved the shield with windows of a given size and studied how the statistics vary as a function of window size. For each set of windows, the mean heat flux was calculated for all windows and the statistics (i.e., mean and standard deviation) were compared to those of the other sets. The standard deviation diminishes slightly when the window size increases from 50 km to 250 km, but remains close to the standard deviation of the individual heat flux values (≈7–9 mW m^{-2}). The standard deviation drops by a factor of 2 for a 500 km window size (≈4 mW m^{-2}). At that scale, variations of bulk crustal heat production are not negligible and are associated with changes of crustal structure and composition (Figure 5). The standard deviation of 4 mW m^{-2} provides an upper bound for the magnitude of Moho heat flux variations.

3.3. Variations of Surface Heat Flux and Traveltime Delays

[27] We have calculated average values of the *S* wave traveltime delay for both the CUB2.0 and the NA04 seismic models over the ten windows (Figure 6). These windows sample the main provinces of the Canadian Shield (Trans-Hudson orogen, Superior, Grenville, Appalachians) (Figure 4). Window A in the Proterozoic Trans-Hudson Orogen contains only areas of juvenile crust, and excludes data from the Thompson belt adjacent to the Superior Province and from the Snow Lake–Flin Flon belt. The former is made of enriched sediments deposited in an ancient continental margin at the western edge of the Superior Province whereas the latter is underlain by radiogenic basement of the small Archean Sask craton [*Rolandone et al.*, 2002]. The Thompson belt is narrow and associated with a local heat flux anomaly that does not affect temperatures deep in the lithosphere. Our window is outside the part of the Trans-Hudson orogen where young kimberlite occurrences have been reported and where seismic tomography suggests that the lithospheric root was thermally perturbed [*Bank et al.*, 1998].

[28] Differences between the two seismic models appear clearly when traveltimes are compared to the heat flux data (Figure 8). The NA04 data for the Archean regions are tightly clustered, in contrast to those from the CUB2.0 model. In both cases, the correlation between surface heat flux and traveltime delay is poor. With the NA04 data, a rough correlation between heat flux and traveltime emerges because of the Appalachian data (window K), which stand out from all the others. *Perry et al.* [2006b] had already noted the lack of correlation between surface heat flux and P_n velocities in the Superior and Grenville Provinces, which they attributed to variations of surface heat flux being mostly of crustal origin.

[29] For the sake of simplicity, we assume that seismic traveltime delay variations record differences of thermal structure in the lithospheric root and that these differences are mostly due to changes of basal heat flux. In this regard, two features of Figure 8 must be noted. One is that we find windows with almost the same traveltime delay over the entire range of heat flux averages. This confirms that surface heat flux variations are not due to lateral temperature changes in the lithospheric mantle and mostly record changes of crustal heat production. The other feature of Figure 8 is that a large range of traveltime delays can be sampled at almost constant surface heat flux (in a 38–44 mW m^{-2} range). Low heat flux values are most appropriate for lithospheric thermal models because the crustal heat production is low and hence does not affect much mantle temperatures. We shall

Table 6. Parameter Values for Geotherms[a]

Parameter	Notation	Value
Upper crust thickness	h_1	9.1 km
Crust thickness	h_2	40 km
Heat production in the lower crust	A_{uc}	0.35 μW m^{-3}
Moho heat flux	Q_m	12–18 mW m^{-2}
Mantle potential temperature	T_{pot}	1350°C
Isentropic gradient	γ	0.5°C.km^{-1}
Upper crustal heat production*	A_{uc}	0.35–2.80 μW m^{-3}
Lithospheric thickness*	H	180–300 km

[a]Asterisks indicate parameters deduced from comparison between surface heat flux and traveltime delays.

show that the large traveltime differences for the Canadian Shield can only be explained by lateral variations of the Moho heat flux.

4. Seismic Traveltimes Depending on the Thermal Structure

[30] To derive constraints on the heat flux at the base of the Canadian Shield, we calculate geotherms that depend on three inputs: the surface heat flux, the basal heat flux and heat production in the lithospheric mantle. Other parameters and rock properties that enter the calculation are set at references values which have been tested previously against independent data [*Perry et al.*, 2006b; *Michaut et al.*, 2007]. A few parameters such as the potential temperature of the well-mixed convecting mantle have been fixed to our best current estimates. One of our goals is to verify that we can obtain a good fit to the data within the available constraints. A full parametric study of all variables involved is beyond the scope of the present paper and we have only verified that the major conclusion, namely that the heat flux at the base of the lithosphere must vary laterally, is not affected by the specific choices that have been made. Each geotherm is converted into a vertical profile of *S* wave seismic velocity, which then allows calculation of the traveltime in the 60–300 km depth interval to compare with the seismic model of *van der Lee and Frederiksen* [2005].

4.1. Calculation Method

[31] We assume that the crust is stratified in two layers, and that the upper crust is enriched in radiogenic elements with respect to the lower crust on average. The input parameters for our model are therefore the surface (Q_s) and Moho (Q_m) heat flux, the thicknesses of the crust (h_2) and of the upper crust (h_1), the upper (A_{uc}) and lower (A_{lc}) crustal heat productions, the mantle heat production (A_m), the potential temperature of the mantle (T_{pot}) as well as the isentropic gradient in the well-mixed convective mantle (γ). We will discuss later the values that have been adopted for

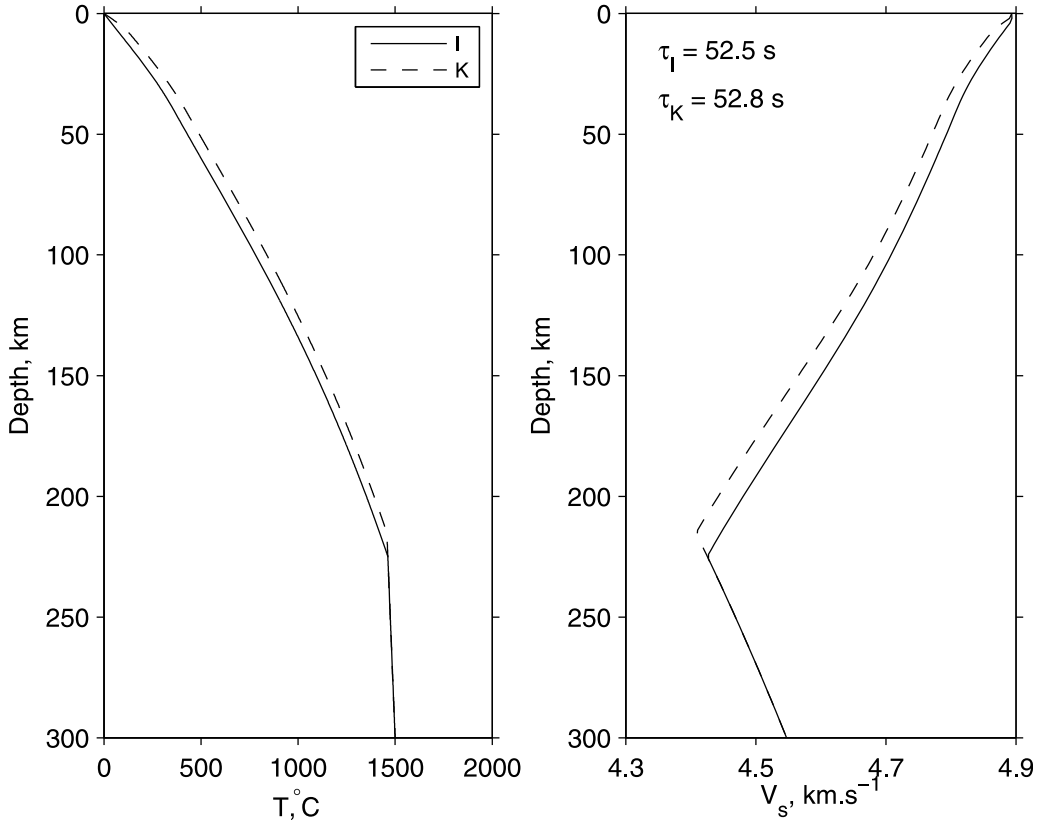

Figure 9. (left) Geotherms and (right) velocity profiles corresponding to the average surface heat flux values of windows I (Q_s = 28.7 mW m^{-2}) and K (Q_s = 57.3 mW m^{-2}). For both windows, the Moho heat flux is fixed at the same value of 15 mW m^{-2}. The other parameter values are summarized in Table 6. τ_I and τ_K are the calculated *S* wave traveltimes over the 60–300 km depth interval.

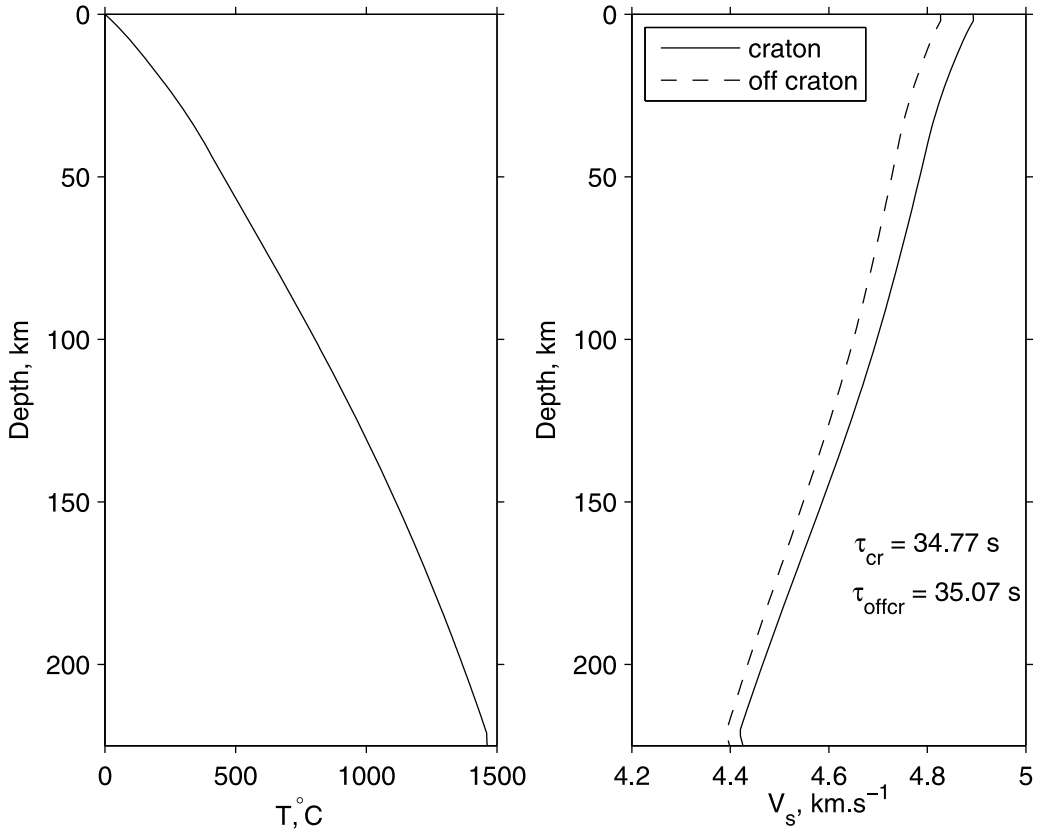

Figure 10. (left) Vertical temperature profile for a 220 km thick lithosphere with zero heat production in the lithospheric mantle, a surface heat flux of 40 mW m^{-2}, and a Moho heat flux of 15 mW m^{-2}. (right) Vertical profiles of *S* wave velocity for two model compositions for the lithospheric mantle, on craton and off craton, from *Goes et al.* [2000].

each parameter. For each layer, we solve the steady state heat conduction equation in a medium with heat production and temperature-dependent thermal conductivity:

$$\frac{\partial Q}{\partial z} = -A(z) \tag{1}$$

$$\frac{\partial T}{\partial z} = \frac{1}{k(T)} Q(z) \tag{2}$$

where $k(T)$ is the thermal conductivity, and the boundary conditions at the surface are $Q(z = 0) = Q_s$ and $T(z = 0) = 0°C$, which is about right for Canada.

[32] We use the temperature-dependent equations for thermal conductivity that are developed in Appendix B. We solve the heat conduction equation down to the depth where the geotherm intersects the mantle isentrope. This provides an estimate of lithosphere thickness. Below the lithosphere, temperature increases linearly along the isentropic gradient. Such profiles are characterized by a discontinuity in temperature gradient at the base of the lithosphere.

[33] We assume an upper crust 9.1 km thick, which is derived from the linear relationship between province-wide-averaged surface heat flux and heat production (Figure 5). The linear relationship itself demonstrates that heat production variations in the lower crust are small across the stable continent. This is also supported by geochemical data from both granulite facies terrains [e.g., *Fountain et al.*, 1987; *Shaw et al.*, 1994] and xenolith suites [*Rudnick and Fountain*, 1995]. Exposed granulites yield values of 0.3 μW m^{-3}, xenoliths lead to 0.4–0.5 μW m^{-3}. For our model, we fix the lower crustal heat production at the mean value of 0.35 μW m^{-3}. For each set of values of surface and Moho heat fluxes, heat production in the upper crust is readily calculated according to the following equation:

$$A_{uc} = \frac{1}{h_1}(Q_s - Q_m - A_{lc}(h_2 - h_1)). \tag{3}$$

Another option would be to assume a homogeneous crustal column. For the low heat flux areas of the Canadian Shield, lithospheric temperatures are not sensitive to crustal stratification. Temperature differences between the homogenous and stratified crustal models are less than 30 K in almost all cases. Using the approximation of a homogeneous crust and allowing for the resulting uncertainty on crustal temperatures, *Perry et al.* [2006b] obtained a good agreement between calculated and observed P_n velocity values in the Superior Province. In this study, we have used two layers in order to compare model results and measured heat production in the surface rocks. Furthermore, a stratified crustal column is required to account for the large changes of crustal structure and composition that occur among the geological provinces of North America.

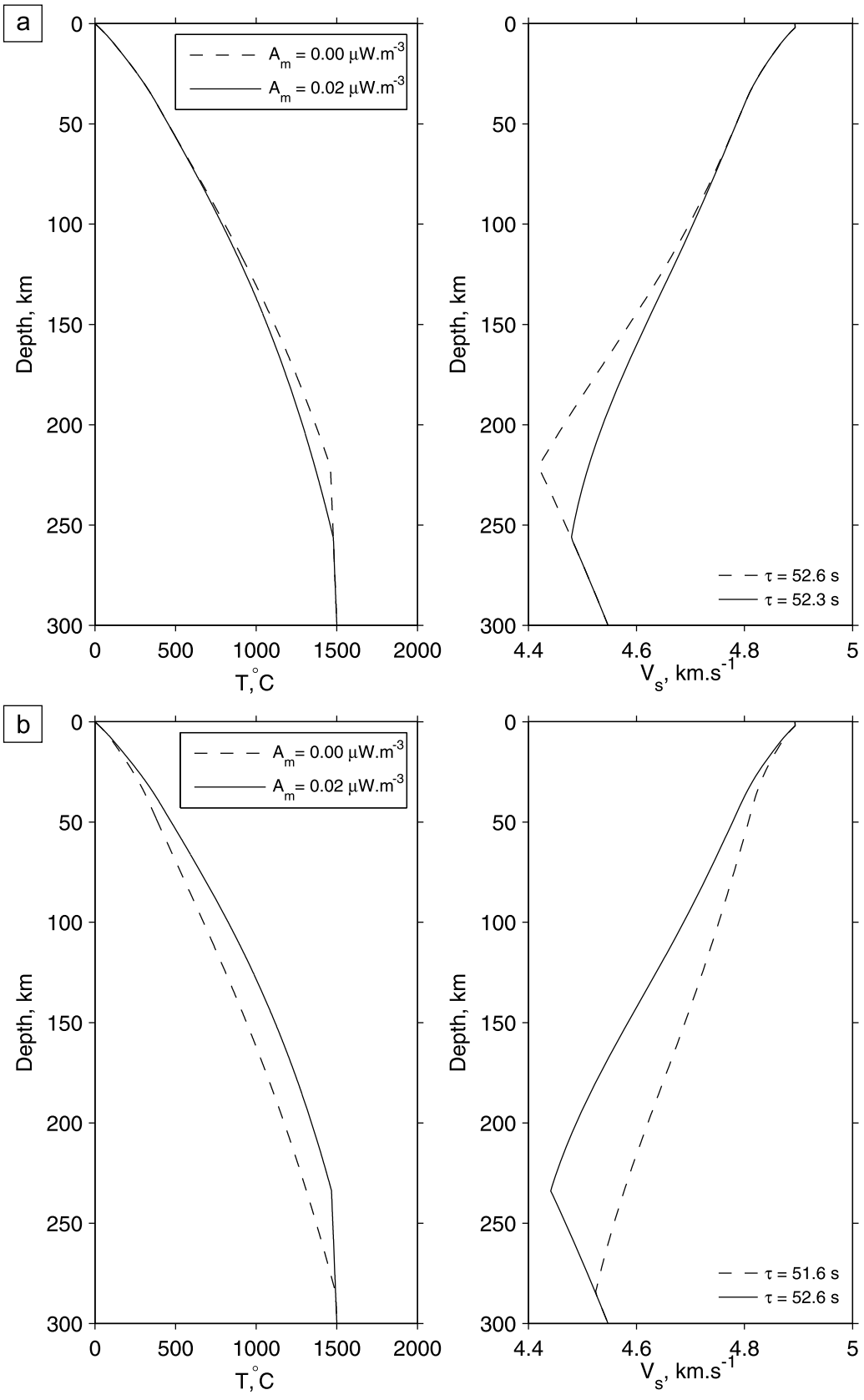

Figure 11. Sensitivity test for thermal models of the lithospheric mantle with different values of heat production for a surface heat flux of 40 mW m^{-2}. (a) Calculations for a fixed Moho heat flux (equal to 15 mW m^{-2}) and hence variable heat flux at the base of the lithosphere. (b) Calculations for a fixed basal heat flux (12 mW m^{-2}) and variable Moho heat flux.

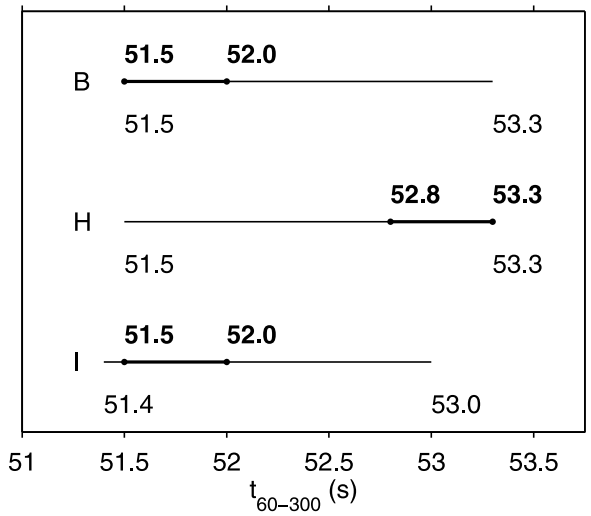

Figure 12. Ranges of calculated traveltime delays for three areas of the Canadian Shield (labels refer to the windows of Figures 3 and 6) for values of the Moho heat flux in a range of 12–18 mW m^{-2}. Thick lines show solutions that are consistent with the NA04 tomographic model. See section 4 for details on calculations and parameters.

[34] Seismic refraction surveys show that the crustal thickness varies across the Canadian Shield [*Perry et al.*, 2002], but there are few crustal thickness data for many parts of the shield including the new heat flux sites. This is not a severe limitation for our study of seismic velocities in the lithosphere deeper than 60 km. For those depths, calculations are weakly sensitive to changes of Moho depth. Save for two small areas around the Kapuskasing uplift and the Keweenawan rift northern termination above Lake Superior, crustal thickness within the Canadian Shield remains within a relatively narrow 38–45 km range. Heat production is low in both the lower crust and the lithospheric mantle, so that changes in the vertical temperature gradient are small immediately above and below the Moho. Allowing for the small change of thermal conductivity between the lower crust and mantle rocks, lateral temperature contrasts due to a change in crustal thickness do not exceed a few tens of degrees. Thus, it is sufficient to assume a uniform Moho depth (which we take to be 40 km). This assumption is not valid for studies of P_n velocity variations, however [*Perry et al.*, 2006b].

[35] The thermal model involves many parameters that remain poorly known, and we restrict ourselves to plausible values for most of them. Thus, the following results should be considered as a subset of a larger set. Values adopted for crustal thickness, heat production in the lower crust, the mantle potential temperature and the isentropic gradient are summarized in Table 6. Constraints on heat production in the lithospheric mantle are weak and have been discussed at length by *Rudnick et al.* [1998] and *Michaut et al.* [2007], and we shall allow for variations in the 0–0.02 μW m^{-3} range. In the model calculations below, therefore, the Moho heat flux is not necessarily equal to the heat flux at the base of the lithosphere. The potential temperature of the convective mantle and the isentropic gradient are assumed to be 1350°C and 0.5 K km^{-1} respectively. Temperature profiles are converted into *S* wave velocity profiles using the parametrization scheme of *Goes et al.* [2000] and *Shapiro et al.* [2004], which is based on laboratory measurements of thermoelastic properties of mantle minerals and models for the average mineralogical composition of the mantle. As appropriate to the study area, we take values for Archean cratonic lithosphere and evaluate the sensitivity of our conclusions to the compositional model. We finally integrate velocity profiles to determine the corresponding traveltime τ:

$$\tau = \int_{z_0}^{z_b} \frac{dz}{v(z)}, \tag{4}$$

where z_0 = 60 km and z_b = 300 km. The seismic models provide traveltime delays with respect to a reference Earth model, and hence are best used for calculations of lateral differences of thermal structure in the Canadian Shield.

4.2. Sensitivity Analysis

[36] We first evaluate the sensitivity of the *S* wave traveltime to the main input parameters for the thermal model.

[37] We have calculated the geotherms for windows I and K which include the extreme heat flux averages in this study (28.7 and 57.3 mW m^{-2}, respectively), with the same value (15 mW m^{-2}) for the Moho heat flux (Figure 9). Despite the large difference of heat flux at the surface, both temperature profiles are very similar and lead to a traveltime difference of about 0.3 s, which is close to the accuracy of the tomographic data and hence can be considered negligible. This is not consistent with the about 2 s difference in traveltime delays between windows I and K (Figure 8 and Table 4). This example shows that variations of crustal heat production are not sufficient to account for the observed seismic traveltime differences. Heat production variations do lead to slight temperature differences at depth, but these differences are too small to account for the seismic data. One could obtain larger differences in mantle temperatures by assuming a vertically uniform distribution of heat producing elements in the crust, but the differences are still too small to account for the traveltime delays. Such solutions would not be consistent with the well-established differentiation of the Appalachian crust in window K.

[38] Figure 10 shows the impact of the compositional model adopted for the lithospheric mantle on the seismic velocities. We have taken the on-craton and off-craton parameters from *Goes et al.* [2000] for an average heat flux of 40 mW m^{-2} and a Moho heat flux of 15 mW m^{-2}, corresponding to a 220 km thick lithosphere. The total traveltime difference between the two models is equal to 0.3 s, which is close to the uncertainty in the traveltime data ($\approx\pm$0.1 s).

[39] We also calculated the effect of heat production in the lithospheric mantle. We fix the surface heat flux at 40 mW m^{-2} and the Moho heat flux Q_m = 15 mW m^{-2} and A_m = 0 or 0.02 μW m^{-3}, such that Q_b = 15 or 10.7 mW m^{-2}. Figure 11a shows that the two temperature profiles are very close to one another and that the resulting traveltime difference is not significant for the current level of uncertainty in the data (0.3 s). In another set of calculations (Figure 11b), we have kept the basal heat flux at the same value of 12 mW m^{-2} and have varied the lithospheric heat production (A_m = 0 and 0.02 μW m^{-3}). This leads to Moho heat flux of 12 and

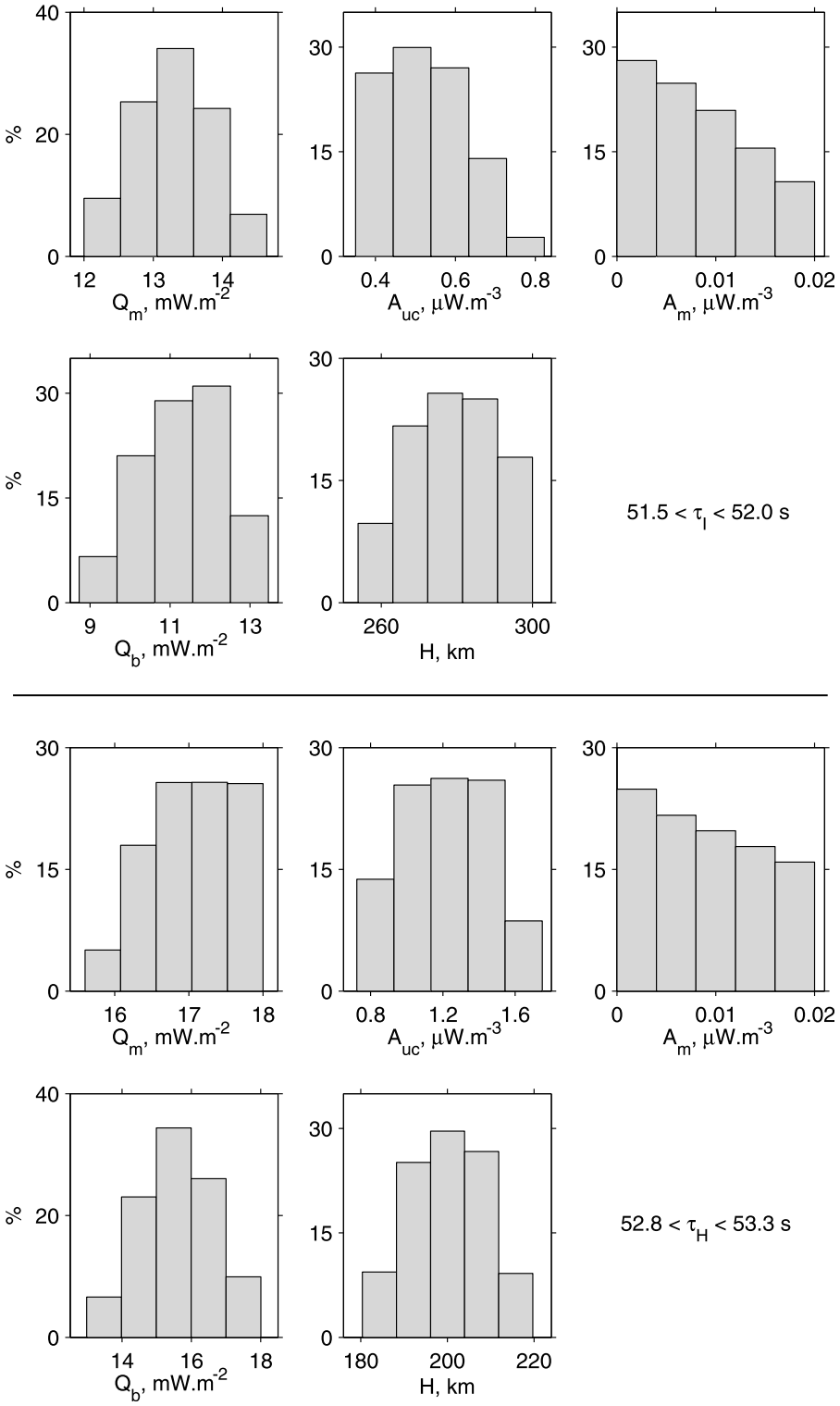

Figure 13. Distribution of parameter values for solutions that are consistent with both surface heat flux and traveltime data for windows (top) I and (bottom) H. The Moho heat flux, heat production in the upper crust and in the mantle, basal heat flux, and lithosphere thickness are shown. Table 7 summarizes the ranges of acceptable values for these variables. The other model parameters are imposed (see Table 6).

15.9 mW m^{-2}. In that case, the temperature profiles begin to diverge at shallow depth, which induces larger thermal contrasts at all depths. As a consequence, the traveltime difference is larger (1 s) and unambiguously above the uncertainty level.

[40] We conclude from all these tests that the traveltimes are weakly sensitive to composition and to heat production in the lithospheric mantle. They are therefore mostly sensitive to the Moho heat flux. Nevertheless, we shall allow

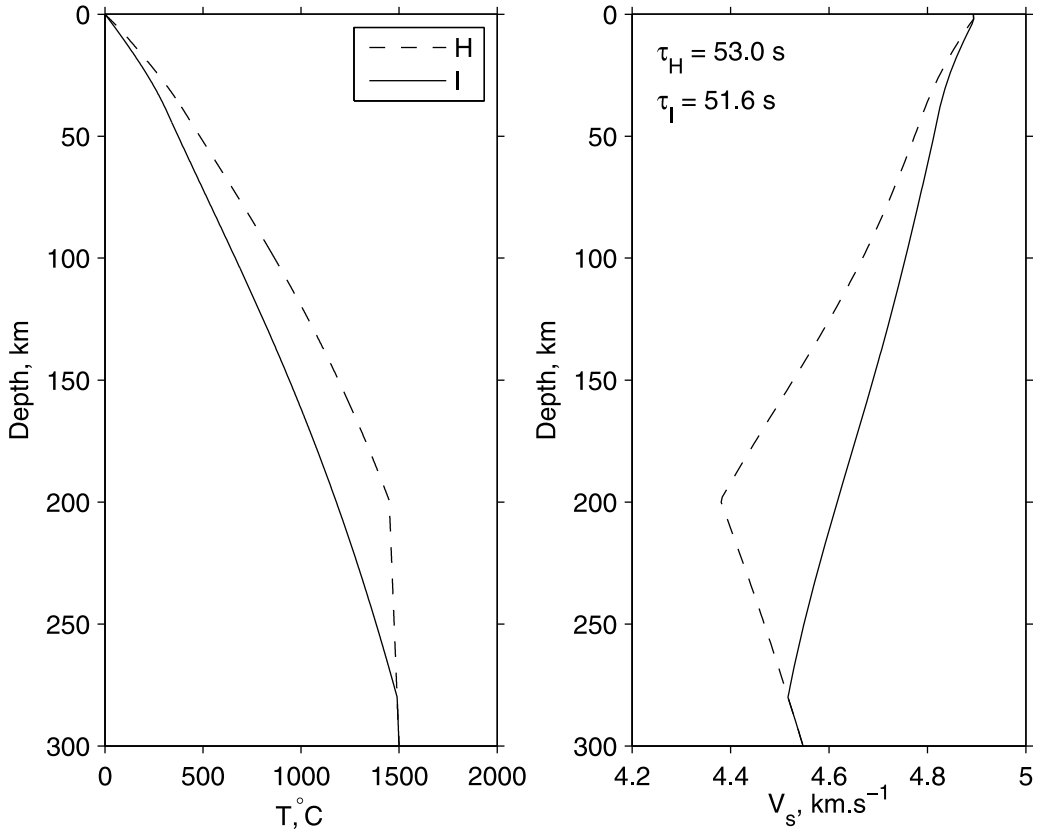

Figure 14. (left) Geotherms and (right) velocity profiles corresponding to the surface heat flux of windows I (Q_s = 28.7 mW m^{-2}) and H (Q_s = 38.9 mW m^{-2}) and consistent with the tomographic model NA04. The Moho heat flux is 12.4 mW m^{-2} for window I and 16.5 mW m^{-2} for window H. The other parameter values are given in Table 6. τ_I and τ_H are the calculated *S* wave traveltimes over a 60–300 km depth interval.

for variations of lithospheric mantle heat production because we are interested in the magnitude of basal heat flux variations.

4.3. Thermal Models That Are Consistent With Heat Flux and Seismic Data

[41] We restrict our analysis to the Canadian Shield proper, and hence do not deal with the Appalachians data in order to avoid the effects of possible thermal transients associated with recent thermal perturbations. We consider windows H and I which span the whole range of traveltime delays. We have also considered window B, for which the traveltime delay is the same as that of window I but the heat flux is larger, in order to evaluate the influence of the heat flux difference. For each window, we consider values of the average surface heat flux that are within one standard error of the mean and we allow the Moho heat flux to vary between 12 and 18 mW m^{-2}. This range is consistent with previous analyses [*Mareschal and Jaupart*, 2004; *Perry et al.*, 2006b] that are briefly reviewed in Appendix C.

[42] We first consider calculations for windows H and I which have a 1.3 s difference in traveltime. Varying the Moho heat flux within the specified 12–18 mW m^{-2} range leads to traveltimes that are between 51.5 and 53.3 s (Figure 12). The longer traveltimes correspond to hotter geotherms and hence to the highest values of the Moho heat flux. We first note that the traveltime difference may be as large as 1.3 s, which is the measured value (Table 4). In order to fit the seismic data, we allow for 0.2 s uncertainty and consider solutions for the highest traveltimes for window H (between 52.8 and 53.3 s) and for the lowest traveltimes for window I (between 51.5 and 52.0 s). The full range of Moho heat fluxes that are consistent with these constraints and with the surface heat fluxes is shown in Figure 13 and is given in Table 7. The Moho heat flux cannot be the same for the two windows as their solution spaces do not overlap. One can see that the combination of heat flux and seismic constraints narrows down the range of solutions, as pointed out on different grounds by *Shapiro et al.* [2004]. Figure 14 shows two vertical profiles of temperature and seismic velocity that are consistent with all available constraints. As discussed above, several parameters have been kept constant in these calculations and may deviate slightly from the chosen values. Exploring the full range of acceptable solutions is postponed to a companion study focussed on mantle parameters. We note, however, that these calculations lead to values of heat production in the upper crust that are consistent with the data. For consistency with traveltime data, the upper crustal heat production must indeed be higher in window H, located in the Proterozoic Grenville Province, than in window I in the Superior Province. As noted above,

Table 7. Output Parameter Values for the Windows Located in the Superior Province and at the Grenville Front, Deduced From Comparison Between Surface Heat Flux Data and Tomographic Traveltime Delays[a]

Window	τ (s)	A_{uc} (μW m^{-3})	Q_m (mW m^{-2})	Q_b (mW m^{-2})	H (km)
B	51.5–52.0	1.82–2.49	12.0–14.3	8.5–13.1	257–300
H	52.8–53.3	0.72–1.75	15.6–18.0	13.0–18.0	180–220
I	51.5–52.0	0.35–0.82	12.0–14.6	8.7–13.5	254–300

[a]For each window, the range of traveltimes τ allowed for consistency with tomography is indicated. A_{uc} is the heat production in the upper crust, Q_m is the Moho heat flux, Q_b is the basal heat flux, and H is the thickness of the lithosphere.

the large-scale average of heat production in the Grenville Province is 0.8 μW m^{-3}, which is within the range of the successful solutions (albeit at the lower end of the range). The same is true for window I.

[43] For completeness, we show in Figure 15 solutions for window B. These solutions have been obtained for traveltimes between 51.5 and 52.0 s (Figure 12). Ranges for the lithosphere thickness and the Moho heat flux are almost identical to those for window I.

[44] The solutions have been obtained for values of the Moho heat flux in a range centered at 15 mW m^{-2}. Such small values imply thick lithosphere, so that variations of traveltime delays can be achieved with relatively small temperature differences distributed over a large vertical distance. We have also derived solutions for higher Moho heat flux, but the spread of values is wider because, in this case, the lithosphere is thin and larger temperature differences are required to achieve the same traveltime differences. For example, we found variations of ±5 mW m^{-2} for the Moho heat flux if the range is centered at 20 mW m^{-2}. Such large variations are not consistent with the systematics of heat flux and heat production in North America.

4.4. Heat Flux at the Base of the Lithosphere

[45] The histograms of Figure 13 indicate a small amount of overlap between the solutions for the heat flux at the base of the lithosphere beneath windows H and I around a value of 13 mW m^{-2}. Variations of the basal heat flux, if they exist, would provide constraints on mantle convection models as well as on the rheology of the subcontinental mantle. For example, one model for heat supply to the lithosphere involves small-scale convection due to the breakdown of an unstable basal thermal boundary layer [*Doin et al.*, 1997; *Jaupart et al.*, 1998; *Solomatov and Moresi*, 2000]. In this case, the heat flux depends on the local value of viscosity in the boundary layer, which increases with the lithospheric thickness due to the pressure dependence of the activation enthalpy. Thus, one expects a relationship between lithosphere thickness and basal heat flux. We note in passing that, due to the large and variable radiogenic heat production of continental crust, the basal heat flux cannot be set equal to a conductive heat flux calculated with a linear temperature gradient through the whole lithosphere. In another model, shear flow associated with horizontal continental motions at the top of the convecting mantle prevents small-scale instabilities and heat is supplied to the lithosphere by conduction from the underlying mantle flow. In yet another model, sporadic mantle plumes bring heat to the lithosphere.

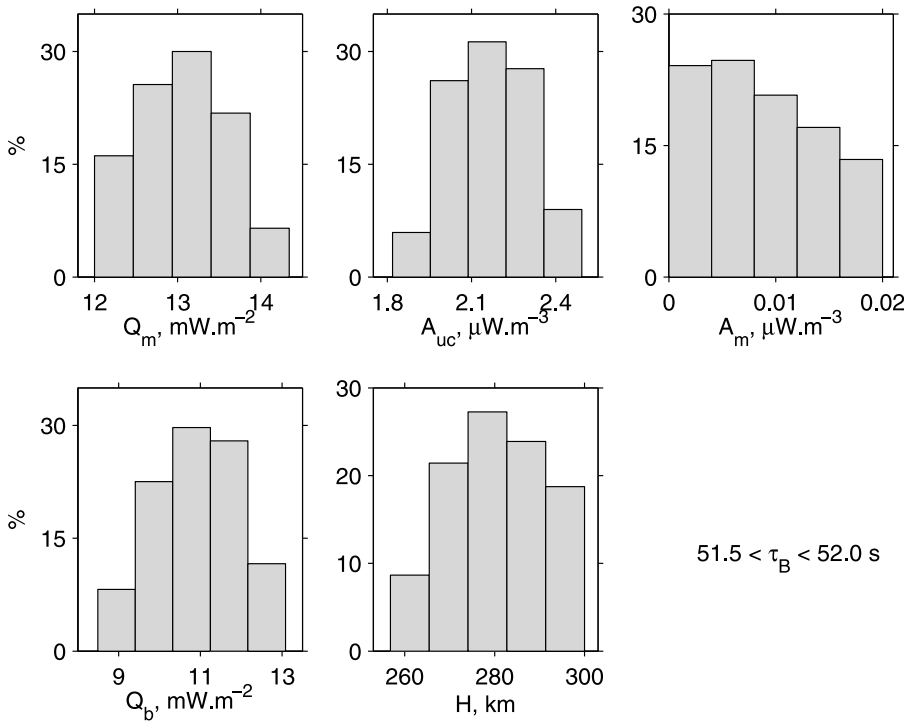

Figure 15. Distribution of parameter values for solutions that are consistent with both surface heat flux and traveltime data for window B. The Moho heat flux, heat production in the upper crust and in the mantle, basal heat flux, and lithosphere thickness are shown. Table 7 summarizes the ranges of acceptable values for these variables. The other model parameters are imposed (see Table 6).

Table 8. Solutions for Windows H and I With Small Variations of Heat Supply at the Base of the Lithosphere[a]

Q_b (mW m^{-2})		A_m (μW m^{-3})		H (km)		
I	H	I	H	I	H	$\Delta\tau_{IH}$ (s)
13.0	13.0	0.00	0.02	264	220	0.9
13.0	13.0	0.01	0.02	240	219	0.4
13.0	13.0	0.01	0.03	240	207	0.7
12.3	13.7	0.00	0.02	282	210	1.3
12.7	13.3	0.00	0.03	271	204	1.3

[a] A_m is the heat production in the lithospheric mantle, $\Delta\tau_{IH}$ is the traveltime difference between the two windows, and other variables are as in Table 7.

Distinguishing between such models may be possible thanks to the systematics of basal heat flux variations and, more specifically, to the existence or absence of a relationship between lithosphere thickness and basal heat flux.

[46] Table 8 lists thermal parameters for the lithosphere beneath windows H and I that are consistent with heat flux data, focusing on solutions with little or no variation of basal heat flux. Restricting values for A_m, the heat production in the lithospheric mantle, to the 0–0.02 μW m^{-3} range, we find that a perfectly constant basal heat flux does not allow a satisfactory fit to the traveltime data. A small lateral variation of 1.4 mW m^{-2} for the basal heat flux is consistent with the seismic data. Such a small difference may not seem significant, and is certainly below the noise level of surface heat flux measurements, but nevertheless represents a 10% variation. It may be possible to reduce the magnitude of basal heat flux variations by appealing to a larger range for A_m (Table 8). We do not believe, however, that such solutions are realistic because they require the lithosphere beneath window I to be entirely devoid of radioactive elements. Were we to consider that A_m cannot be smaller than some threshold value, such as 0.01 μW m^{-3}, say, we would find no acceptable solutions (Table 8).

[47] It is worth noting that, although the basal heat flux is not well resolved, the lithosphere thickness is. The lithosphere thickness beneath the Superior Province must be 280 ± 20 km and must be significantly smaller beneath the Grenville Province.

4.5. Discussion

[48] We do not report calculations for all the windows of Figure 3 because they would entail local analyses of crustal structure and heat production that are beyond the scope of this study. Thus, we only comment on our results briefly. The lithospheric models obtained above for three regions of the Canadian Shield suggest that the lithosphere thickness varies by about 80 km across the study area. In the Superior Province, the lithosphere is thick (≈280 km) and the small range of traveltime delays that are observed (Figure 6) support only weak variations of lithosphere thickness there. The smallest traveltime delay is found beneath window D where the heat flux is very low. Within the parameter range of the solutions, one may consider constant lithosphere thickness with changes of heat production in the lithospheric mantle or vice versa. Thinner lithosphere seems to underlie the Grenville Province (≈200 km). The solutions further suggest small variations of heat flux at the Moho (≈±3 mW m^{-2}) and at the base of the lithosphere (≈±4 mW m^{-2}), in agreement with the analysis of surface heat flux and heat production data.

[49] The amplitude of basal heat flux variations derived here must be understood as spatial and temporal averages. Variations of heat supply at the base of the lithosphere are efficiently smoothed out by diffusion and leave a very damped signal in the surface heat flux. Through ~250 km thick Archean lithosphere, wavelengths less than 1000 km are strongly attenuated and all wavelengths shorter than 500 km are effectively eliminated [*Mareschal and Jaupart*, 2004]. Thus, variations that have been documented must be considered as part of a larger-scale pattern. Surface heat flux is not affected by recent changes of basal heat flux and, for 200 km thick lithosphere, variations on a time scale of less than 300 Myr are never seen at the surface. Thus, our results must be understood as long-term averages.

5. Conclusions

[50] Combined with the seismic traveltime data, surface heat flux measurements allow precise models of lithospheric structure. Heat flux data provide constraints on the basal heat flux and temperature that would be impossible to derive from seismic observations alone. They potentially allow discrimination between temperature and composition effects on seismic velocities, although this was not necessary for the Precambrian lithosphere of this study.

[51] New surface heat flux determinations define a large zone of very low heat flux in the north-central part of the Superior Province. Combining the heat flux data set which now covers most of the shield south of 54°N, with S wave traveltime delays allows calculation of temperature in the lithospheric mantle. We find that the Moho heat flux is not uniform beneath the shield. Its variations are limited in amplitude (±3 mW m^{-2} around a mean value of 15 mW m^{-2}) but the differences in temperature profiles imply a variable lithospheric thickness. Variations of the basal heat flux are constrained to be smaller than 8 mW m^{-2}. Solutions for a laterally uniform basal heat flux are only achieved for a value of about 13 mW m^{-2}. Further improvements on the deep thermal structure of continental lithosphere will require tight constraints on heat production in the lithospheric mantle.

Appendix A: Measurement Techniques

A1. Heat Flux

[52] The surface heat flux is determined from measurements of the temperature gradient in boreholes and the conductivity of rock samples:

$$Q = k\frac{\partial T}{\partial z} \tag{A1}$$

where k is the thermal conductivity in the vertical direction, T is temperature, and z is depth.

[53] Heat flux was determined from mining exploration boreholes. Recent climate changes and surface perturbations can affect temperatures at shallow depth and yield a non-equilibrium temperature profile. To avoid this problem, we try to find boreholes that are deeper than 300 m and we never make measurements in holes less than 200 m deep.

Whenever possible, we acquire data from several neighboring holes.

[54] Temperature is measured at depth intervals of ten meters with a thermistor probe calibrated in the laboratory to 0.005 K accuracy. Thermal conductivity is determined at regular intervals of ≈80 m and at each lithological discontinuity. Some of the heavily deformed rocks of the province may be anisotropic and many of the boreholes used in this work deviate from the vertical. To account for anisotropy, we measure conductivity in the vertical direction through small disks that are cut from long core samples. For each sample, five disks of different thicknesses are prepared (thickness from 2 to 10 mm). The thermal resistance of each disk is measured with a divided bar apparatus, and thermal conductivity is calculated by a least squares linear fit to the resistance/thickness data. This procedure eliminates sample-scale heterogeneities and yields conductivity values representative of the large-scale average rock composition. Multiple calibrations allow measurement accuracy to be greater than 3%.

[55] We correct the heat flux values for climatic effects due to the retreat of the Laurentide ice sheet between 12 and 9 ka. The climatic correction depends on the site location and follows the model of *Jessop* [1971]. This model includes all the surface temperature variations from 400 ka to present. It is assumed that surface temperature at the base of the ice sheet is equal to the melting temperature of ice, and that the temperature during the interglacial periods was the same as present. Present surface temperature is changing, as shown by the curvature of many temperature profiles. The reference surface temperature is determined by upward continuation to the surface of the deepest segment of the temperature profile. Temperature measurements in very deep boreholes have confirmed that the post glacial correction is small over most of Canada and that the temperature at the base of the Laurentian glacier was near melting [*Chouinard and Mareschal*, 2009].

[56] Sites are rated A, B or C following the guidelines established by *Pinet et al.* [1991]. Sites rated A consist of either several boreholes deeper than 300 m or a single borehole deeper than 600 m and where the heat flux is stable over more than 300 m. Sites where the heat flux is less consistent between boreholes or where the heat flux is obtained from a single borehole shallower than 600 m are rated B. Sites consisting of shallow (<300 m) boreholes or where the difference in heat flux between boreholes is larger than two standard deviations are rated C.

A2. Heat Production

[57] Heat production is estimated from the abundance of the main radioactive elements, U, Th and K in core samples, as described by *Mareschal et al.* [1989]. For each site, we report the average heat production of samples from the main geological unit collected in all the available boreholes. Analytical errors on heat production measurements are <5% and are largest for low-radioactivity levels.

Appendix B: Thermal Conductivity

[58] Over the range of crustal temperatures, thermal conductivity can vary by as much as 50%. From laboratory measurements on samples from the Superior Province, *Durham et al.* [1987] derived a relationship between thermal diffusivity, temperature, and the quartz content of rocks. Assuming constant density and specific heat throughout the crust, *Rolandone et al.* [2002] used these results to derive the following relationship between the lattice thermal conductivity and the temperature:

$$k_c(T) = 2.26 - \frac{618.241}{T} + k_o\left(\frac{355.576}{T} - 0.30247\right) \qquad \text{(B1)}$$

where T is absolute temperature and k_o is the thermal conductivity at surface conditions (T = 273 K). We took k_o = 3 W m^{-1}K^{-1} for crustal rocks, which leads to an average conductivity of about 2.5 W m^{-1}K^{-1} over the temperature range of the crust. Including the increase of the specific heat with temperature would result in less variation and slightly higher values of the average crustal thermal conductivity.

[59] In the mantle, one must allow for the radiative component of the thermal conductivity and the effect of pressure. The main constituent of mantle rocks is olivine and several experimental studies are available. *Xu et al.* [2004] have summarized their new measurements and older ones and have shown that the lattice conductivity of olivine is such that:

$$k_L(T,P) = k_{298}\left(\frac{298}{T}\right)^{1/2}(1 + 0.032P) \qquad \text{(B2)}$$

where k_{298} is conductivity at T = 298 K and atmospheric pressure, and P is pressure in GPa. k_{298} is 4.13 ± 0.11 W m^{-1}K^{-1} for Fo_{90} and ≈4.7 W m^{-1}K^{-1} for pure forsterite. At temperatures less than 700 K, radiative transfer can be neglected [*Shankland et al.*, 1979]. At higher temperatures, laboratory measurements by *Schatz and Simmons* [1972], *Beck et al.* [1978], and *Schärmeli* [1979] have led to the approximate relationship:

$$k_r = 0.368 \times 10^{-9}T^3 \qquad \text{(B3)}$$

This relation is only valid in a single crystal if the mean free path of photons is independent of temperature. For mantle rocks, one must account for scattering and for the effect of interfaces in a mineral assemblage. Such complications led *Marton et al.* [2005] to use a constant radiative conductivity component k_r = 1 W m^{-1}K^{-1} for temperatures larger than 700 K. *Gibert et al.* [2005], however, have found that the conductivity of polycrystalline dunite samples conforms to relation (B3) and is close to that of single olivine crystals. For 700 < T < 1700 K, which is the range of interest for thick lithospheric roots, equation (B3) leads to 0.13 < k_r < 1.8 W m^{-1}K^{-1} which is close to the approximation of a constant k_r at a value of 1 W m^{-1}K^{-1}. *Gibert et al.* [2005] have proposed conductivity values that are significantly higher than those of earlier studies. The effect of pressure on the radiative conductivity component is negligible.

[60] Archean and Proterozoic provinces are associated with lithospheric mantles of different compositions [*Griffin et al.*, 2003]. Differences are essentially in the Cpx, Opx and olivine contents. The thermal conductivities of olivine and orthopyroxene differ by about 30% [*Schatz and Simmons*, 1972]. Changes in the amounts of these two minerals are complementary to one another, so that the net effect on the bulk rock conductivity is small (≈0.1 W m^{-1}K^{-1}). In fact,

the slight differences of olivine composition that exist between the two types of mantle (between about Fo_{92} and Fo_{90}) have an opposite effect on the bulk conductivity. Lack of data on clinopyroxene prevent a comprehensive calculation, but the resulting uncertainty is negligible for such a minor constituent. Thus, we do not expect significant differences of thermal structure between Archean and Proterozoic provinces due to changes of thermal conductivity.

Appendix C: Variations of the Moho Heat Flux

[61] Here we briefly review data that have been used to determine the Moho heat flux and its variations across the Canadian Shield.

[62] Xenolith samples from kimberlite pipes allow estimates of pressure and temperature within the lithospheric mantle and hence estimates of the mantle heat flux. For the Kirkland Lake pipe, within the Superior Province, *Rudnick and Nyblade* [1999] obtained a best fit Moho heat flux estimate of ≈18 mW m^{-2} within a total range of 17–25 mW m^{-2}. The recent experimental work summarized in Appendix B leads to conductivity values that are slightly smaller than those used by *Rudnick and Nyblade* [1999]. In such conditions, for a given temperature gradient deduced from (P,T) xenolith data, the predicted heat flux is slightly enhanced. Further, *Rudnick and Nyblade* [1999] forced the surface heat flux to lie within a (35–39) mW m^{-2} range, whereas a reliable measurement at the same location (Kirkland Lake) gives a value of 42 mW m^{-2} [*Jessop and Lewis*, 1978]. The various input parameters chosen by *Rudnick and Nyblade* [1999] are close to those we would use today, but are responsible for small differences of a few mW m^{-2} in estimates of the Moho heat flux. With a similar approach but a different thermal conductivity model, *Russell et al.* [2001] derived a best fitting value of 15 mW m^{-2}, within a range between 12–24 mW m^{-2}, for the Jericho kimberlite area of the Archean Slave Province, about 1000 km west of the Trans-Hudson Orogen. In the Lac de Gras kimberlite pipes, which also belong to the Slave province, surface heat flux data are available and allow tighter constraints of 12–15 mW m^{-2} for Q_m [*Mareschal et al.*, 2004].

[63] Another method relies on the variations of heat flux and crustal structure combined with heat production data for the various rock types. Moho heat flux values of 10–15 mW m^{-2} have thus been derived for the Grenville Province, east of the western Superior [*Pinet et al.*, 1991], and for the Trans-Hudson Orogen (THO) to the west [*Rolandone et al.*, 2002]. A key point is that, over a single geological province such as the Abitibi belt for example, the Moho heat flux cannot change significantly, for reasons that have been detailed in section 3.2. Thus, surface heat flux variations can only be due to changes of crustal heat production, which can be related to other geophysical data on crustal structure. Gravity data have been used to further constrain lateral variations of crustal structure [*Guillou et al.*, 1994]. Crustal models are generated by varying the Moho heat flux, the thicknesses of the lithological units, their densities and heat production rates. In the Abitibi belt of the Superior Province, only a limited number of models meet the constraints of both gravity and heat flux data, with values of Q_m lying between 7 and 15 mW m^{-2} [*Guillou et al.*, 1994].

[64] Yet another method relies on a comparison between calculated Moho temperatures and values of P_n velocities from seismic refraction surveys. For depleted mantle compositions appropriate to the Superior Province, a good fit between predicted and observed P_n velocity values is obtained if the Moho heat flux is within a range of 12–25 mW m^{-2} [*Perry et al.*, 2006b]. These different and independent methods have all been applied to data from the Abitibi belt and can be combined to tighten the final range to 12–15 mW m^{-2} for that subprovince.

[65] Lower and upper bounds on the Moho heat flux can be derived using other arguments. *Rolandone et al.* [2002] calculated lower crustal temperatures when different provinces of the Canadian Shield stabilized, which depend on the crustal heat production. Requiring that temperatures were below melting, they found that Q_m could not be less than about 12 mW m^{-2}. Upper bounds on the mantle heat flux are provided by the lowest heat flux measured in the shield. Values of 20–23 mW m^{-2} have been found throughout the shield, from the Trans-Hudson Orogen to the eastern edge in Labrador [*Mareschal et al.*, 2000]. One can refine this estimate to 18 mW m^{-2} using lower bounds on crustal heat production.

[66] The various methods described above rely on different data and hence are associated with different sources of uncertainty. That such completely independent methods converge to similar results allows some confidence in the final range obtained. Values smaller than 12 mW m^{-2} are not consistent with the xenolith data whereas values larger than 18 mW m^{-2} can be excluded because of the heat flux data. This upper bound appears to be valid for the whole shield.

[67] One final constraint is provided by the observed correlation between the average surface heat flux and heat production for five large provinces of the Canadian shield [*Perry et al.*, 2006a]. If there were large variations of the Moho heat flux, they would need to be compensated by opposite variations of the average lower crustal heat production. To our knowledge, no physical mechanism can explain how such independent variables can be linked to one another. Variations of the Moho heat flux are therefore limited by the magnitudes of the intrinsic uncertainty of the heat flux measurement technique and by the magnitude of departures from the heat flux–heat production relationship, which is about 2–3 mW m^{-2} [*Mareschal and Jaupart*, 2004]. We therefore conclude that the Moho heat flux must lie within a range of 12–18 mW m^{-2} beneath the Canadian Shield.

[68] **Acknowledgments.** We thank Christian Chouinard for help with measurements in the field beyond the call of duty and Raynald Lapointe for the impeccable logistics. Nikolai Shapiro provided us with the *S* wave traveltimes and the function specifying the *S* wave velocity dependence on temperature and pressure. Comments by three anonymous reviewers and the Associate Editor led to substantial improvements. This study was supported by ANR, France (contract BegDy). J.-C.M. is grateful to NSERC (Canada) for its continuous support.

References

Artemieva, I., and W. Mooney (2001), Thermal thickness and evolution of Precambrian lithosphere: A global study, *J. Geophys. Res.*, *106*, 16,387–16,414.

Bank, C.-G., M. G. Bostock, R. M. Ellis, Z. Hajnal, and J. C. VanDecar (1998), Lithospheric mantle structure beneath the Trans-Hudson Orogen

and the origin of diamondiferous kimberlites, *J. Geophys. Res.*, *103*, 10,103–10,114, doi:10.1029/97JB03746.

Beck, A. E., D. M. Dharba, and H. H. Schloessin (1978), Lattice conductivities of single crystal and polycrystalline materials at mantle pressures and temperatures, *Phys. Earth Planet. Inter.*, *17*, 35–53, doi:10.1016/0031-9201(78)90008-0.

Blackwell, D., and M. Richards (2004), Geothermal map of North America, Am. Assoc. Pet. Geol., Tulsa, Okla.

Card, K. D. (1990), A review of the Superior Province of the Canadian Shield, a product of Archean accretion, *Precambrian Res.*, *48*, 99–156.

Chouinard, C., and J. Mareschal (2009), Ground surface temperature history in southern Canada: Temperatures at the base of the laurentide ice sheet and during the Holocene, *Earth Planet. Sci. Lett.*, *277*, 280–289, doi:10.1016/j.epsl.2008.10.026.

Chouinard, C., R. Fortier, and J.-C. Mareschal (2007), Recent climate variations in the subarctic inferred from three borehole temperature profiles in northern Quebec, Canada, *Earth Planet. Sci Lett.*, *263*, 355–369, doi:10.1016/j.epsl.2007.09.017.

Doin, M. P., L. Fleitout, and U. R. Christensen (1997), Mantle convection and stability of depleted and undepleted continental lithosphere, *J. Geophys. Res.*, *102*, 2771–2787, doi:10.1029/96JB03271.

Durham, W. B., V. V. Mirkovich, and H. C. Heard (1987), Thermal diffusivity of igneous rocks at elevated pressure and temperature, *J. Geophys. Res.*, *92*, 11,615–11,634, doi:10.1029/JB092iB11p11615.

Eade, K. E., and W. F. Fahrig (1971), Geochemical evolutionary trends of continental plates: A preliminary study of the Canadian Shield, *Bull. Geol. Surv. Can.*, *179*, 1–59.

Fountain, D. M., M. H. Salisbury, and K. P. Furlong (1987), Heat production and thermal conductivity of rocks from the Pikwitonei-Sachigo continental cross-section, central Manitoba: Implications for the thermal structure of Archean crust, *Can. J. Earth Sci.*, *24*, 1583–1594.

Gibert, B., F. R. Schilling, K. Gratz, and A. Tommasi (2005), Thermal diffusivity of olivine single crystals and a dunite at high temperature: Evidence for heat transfer by radiation in the upper mantle, *Phys. Earth Planet. Inter.*, *151*, 129–141, doi:10.1016/j.pepi.2005.02.003.

Goes, S., and S. van der Lee (2002), Thermal structure of the North American uppermost mantle inferred from seismic tomography, *J. Geophys. Res.*, *107*(B3), 2050, doi:10.1029/2000JB000049.

Goes, S., R. Govers, and P. Vacher (2000), Shallow mantle temperatures under Europe from P and S wave tomography, *J. Geophys. Res.*, *105*, 11,153–11,170, doi:10.1029/1999JB900300.

Griffin, W. L., S. Y. O'Reilly, N. Abe, S. Aulbach, R. M. Davies, N. J. Pearson, B. J. Doyle, and K. Kivi (2003), The origin and evolution of Archean lithospheric mantle, *Precambrian Res.*, *127*, 19–41, doi:10.1016/S0301-9268(03)00180-3.

Guillou, L., J.-C. Mareschal, C. Jaupart, C. Gariépy, G. Bienfait, and R. Lapointe (1994), Heat flow, gravity and structure of the Abitibi belt, Superior Province, Canada: Implications for mantle heat flow, *Earth Planet. Sci. Lett.*, *122*, 103–123, doi:10.1016/0012-821X(94)90054-X.

Hoffman, P. F. (1989), Precambrian geology and tectonic history of North America, in *The Geology of North America—An Overview*, vol. A, edited by A. W. Bally and A. R. Palmer, pp. 447–512, Geol. Soc. of Am., Boulder, Colo.

Jaupart, C., and J. C. Mareschal (2003), Constraints on crustal heat production from heat flow data, in *Treatise on Geochemistry*. vol. 3, *The Crust*, edited by R. L. Rudnick, pp. 65–84, Elsevier, Amsterdam.

Jaupart, C., J. C. Mareschal, L. Guillou-Frottier, and A. Davaille (1998), Heat flow and thickness of the lithosphere in the Canadian Shield, *J. Geophys. Res.*, *103*, 15,269–15,286, doi:10.1029/98JB01395.

Jessop, A. (1971), The distribution of glacial perturbation of heat flow in Canada, *Can. J. Earth Sci.*, *8*, 162–166.

Jessop, A. M., and T. J. Lewis (1978), Heat flow and heat generation in the Superior province of the Canadian Shield, *Tectonophysics*, *50*, 55–57, doi:10.1016/0040-1951(78)90199-3.

Jones, A. G., P. Lezaeta, I. J. Ferguson, A. D. Chave, R. L. Evans, X. Garcia, and J. Spratt (2003), The electrical structure of the Slave craton, *Lithos*, *71*, 505–527.

Mareschal, J. C., and C. Jaupart (2004), Variations of surface heat flow and lithospheric thermal structure beneath the North American craton, *Earth Planet. Sci. Lett.*, *223*, 65–77, doi:10.1016/j.epsl.2004.04.002.

Mareschal, J. C., C. Pinet, C. Gariépy, C. Jaupart, G. Bienfait, G. Dalla-Coletta, J. Jolivet, and R. Lapointe (1989), New heat flow density and radiogenic heat production data in the Canadian Shield and the Quebec Appalachians, *Can. J. Earth Sci.*, *26*, 845–852.

Mareschal, J. C., C. Jaupart, L. Z. Cheng, F. Rolandone, C. Gariépy, G. Bienfait, L. Guillou-Frottier, and R. Lapointe (1999), Heat flow in the Trans-Hudson Orogen of the Canadian Shield: Implications for Proterozoic continental growth, *J. Geophys. Res.*, *104*, 29,007–29,024, doi:10.1029/1998JB900209.

Mareschal, J. C., A. Poirier, F. Rolandone, G. Bienfait, C. Gariépy, R. Lapointe, and C. Jaupart (2000), Low mantle heat flow at the edge of the North American continent Voisey Bay, Labrador, *Geophys. Res. Lett.*, *27*, 823–826, doi:10.1029/1999GL011069.

Mareschal, J. C., A. Nyblade, H. K. C. Perry, C. Jaupart, and G. Bienfait (2004), Heat flow and deep lithospheric thermal structure at Lac de Gras, Slave Province, Canada, *Geophys. Res. Lett.*, *31*, L12611, doi:10.1029/2004GL020133.

Marton, F. C., T. J. Shankland, D. C. Rubie, and Y. Xu (2005), Effects of variable thermal conductivity on the mineralogy of subducting slabs and implications for mechanisms of deep earthquakes, *Phys. Earth Planet. Inter.*, *149*, 53–64, doi:10.1016/j.pepi.2004.08.026.

Michaut, C., C. Jaupart, and D. R. Bell (2007), Transient geotherms in Archean continental lithosphere: New constraints on thickness and heat production of the subcontinental lithospheric mantle, *J. Geophys. Res.*, *112*, B04408, doi:10.1029/2006JB004464.

Pedersen, H. A., S. Fishwick, and D. B. Snyder (2008), A comparison of cratonic roots through consistent analysis of seismic surface waves, *Lithos*, *109*, 81–95, doi:10.1016/j.lithos.2008.09.016.

Perry, H. K. C., D. W. S. Eaton, and A. M. Forte (2002), A revised crustal model for Canada based on Lithoprobe results, *Geophys. J. Int.*, *150*, 285–294.

Perry, H. K. C., C. Jaupart, J.-C. Mareschal, and G. Bienfait (2006a), Crustal heat production in the Superior Province, Canadian Shield, and in North America inferred from heat flow data, *J. Geophys. Res.*, *111*, B04401, doi:10.1029/2005JB003893.

Perry, H. K. C., C. Jaupart, J.-C. Mareschal, and N. M. Shapiro (2006b), Upper mantle velocity-temperature conversion and composition determined from seismic refraction and heat flow, *J. Geophys. Res.*, *111*, B07301, doi:10.1029/2005JB003921.

Pinet, C., C. Jaupart, J.-C. Mareschal, C. Gariepy, G. Bienfait, and R. Lapointe (1991), Heat flow and structure of the lithosphere in the eastern Canadian Shield, *J. Geophys. Res.*, *96*, 19,941–19,963, doi:10.1029/91JB01020.

Pollack, H. N., and D. S. Chapman (1977), On the regional variation of heat flow, geotherms and thickness of the lithosphere, *Tectonophysics*, *38*, 279–296.

Priestley, K., and D. McKenzie (2006), The thermal structure of the lithosphere from shear-wave velocities, *Earth Planet. Sci. Lett.*, *244*, 285–301, doi:10.1016/j.epsl.2006.01.008.

Rohm, A. H. E., R. Snieder, S. Goes, and J. Trampert (2000), Thermal structure of continental upper mantle inferred from S-wave velocity and surface heat flow, *Earth Planet. Sci. Lett.*, *181*, 395–407, doi:10.1016/S0012-821X(00)00209-0.

Rolandone, F., C. Jaupart, J. C. Mareschal, C. Gariépy, G. Bienfait, C. Carbonne, and R. Lapointe (2002), Surface heat flow, crustal temperatures and mantle heat flow in the Proterozoic Trans-Hudson Orogen, Canadian Shield, *J. Geophys. Res.*, *107*(B12), 2341, doi:10.1029/2001JB000698.

Rudnick, R. L., and D. M. Fountain (1995), Nature and composition of the continental crust: A lower crustal perspective, *Rev. Geophys.*, *33*(3), 267–309, doi:10.1029/95RG01302.

Rudnick, R. L., and S. Gao (2003), Composition of the continental crust, in *Treatise on Geochemistry*, vol. 3, *The Crust*, edited by R. L. Rudnick, pp. 1–64, Elsevier, Amsterdam.

Rudnick, R. L., and A. A. Nyblade (1999), The thickness of Archean lithosphere: Constraints from xenolith thermobarometry and surface heat flow, in *Mantle Petrology: Field Observations and High Pressure Experimentation: A Tribute to Francis R. (Joe) Boyd*, edited by Y. Fei, C. M. Bertka, and B. O. Mysen, *Spec. Publ. Geochem. Soc.*, *6*, 3–11.

Rudnick, R. L., W. F. McDonough, and R. J. O'Connell (1998), Thermal structure, thickness and composition of continental lithosphere, *Chem. Geol.*, *145*, 395–411.

Russell, J. K., G. M. Dipple, and M. G. Kopylova (2001), Heat production and heat flow in the mantle lithosphere, Slave craton, Canada, *Phys. Earth Planet. Inter.*, *123*, 27–44.

Schärmeli, G. (1979), Identification of radioactive thermal conductivity in olivine up to 25 kbar and 1500 K, paper presented at 6th AIRAPT Conference, Int. Assoc. for Res. and Adv. of High Pressure Sci. and Technol., Boulder, Colo.

Schatz, J. F., and G. Simmons (1972), Thermal conductivity of Earth materials at high temperatures, *J. Geophys. Res.*, *77*, 6966–6983, doi:10.1029/JB077i035p06966.

Shankland, T. J., U. Nitsan, and A. G. Duba (1979), Optical absorption and radiative heat transport in olivine at high temperature, *J. Geophys. Res.*, *84*, 1603–1610, doi:10.1029/JB084iB04p01603.

Shapiro, N. M., and M. H. Ritzwoller (2002), Monte-Carlo inversion for a global shear-velocity model of the crust and upper mantle, *Geophys. J. Int.*, *151*, 88–105, doi:10.1046/j.1365-246X.2002.01742.x.

Shapiro, N. M., M. H. Ritzwoller, J. C. Mareschal, and C. Jaupart (2004), Lithospheric structure of the Canadian Shield inferred from inversion of

surface-wave dispersion with thermodynamic a priori constraints, in *Geological Prior Information: Informing Science and Engineering*, edited by A. Curtis and R. Wood, *Geol. Soc. Spec. Publ.*, *239*, 175–194.

Shaw, D. M., A. P. Dickin, H. Li, R. H. McNutt, H. P. Schwarcz, and M. G. Trscott (1994), Crustal geochemistry in the Wawa-Foleyet region, Ontario, *Can. J. Earth. Sci.*, *31*, 1104–1121.

Solomatov, V. S., and L. N. Moresi (2000), Scaling of time-dependent stagnant lid convection: Application to small-scale convection on Earth and other terrestrial planets, *J. Geophys. Res.*, *105*, 21,795–21,817, doi:10.1029/2000JB900197.

Taylor, A., and A. S. Judge (1979), Permafrost studies in northern Quebec, *Geogr. Phys. Quat.*, *33*, 245–251.

Thurston, P. C. (2002), Autochtonous development of Superior Province greenstone belts?, *Precambrian Res.*, *115*, 11–36.

van der Lee, S., and A. Frederiksen (2005), Surface wave tomography applied to the North American upper mantle, in *Seismic Earth: Array Analysis of Broadband Seismograms*, *Geophys. Monogr. Ser.*, vol. 157, edited by A. Levander and G. Nolet, pp. 67–80, AGU, Washington, D. C.

van der Lee, S., and G. Nolet (1997), Upper mantle S velocity structure of North America, *J. Geophys. Res.*, *102*, 22,815–22,838, doi:10.1029/97JB01168.

Wickens, A., and G. Buchbinder (1980), S-wave residuals in Canada, *Bull. Seism. Soc. Am.*, *70*, 809–822.

Xu, Y., T. J. Shankland, S. Linhardt, D. C. Rubie, F. Langenhorst, and K. Klasinski (2004), Thermal diffusivity and conductivity of olivine, wadsleyite and ringwoodite to 20 GPa and 1373 K, *Phys. Earth Planet. Inter.*, *143–144*, 321–336, doi:10.1016/j.pepi.2004.03.005.

G. Bienfait, C. Jaupart, F. Lévy, and A. Limare, Équipe de Dynamique des Fluides Géologiques, Institut de Physique du Globe de Paris, Tour 14-15, 4 pl. Jussieu, F-75252 Paris CEDEX 05, France. (levy@ipgp.fr)

J.-C. Mareschal, GEOTOP, Université du Québec à Montréal, POB 8888, Sta. "Downtown," Montréal, QC H3C 3P8, Canada. (mareschal.jean-claude@uqam.ca)